

2(mix)

CR 114489
Available to the Public

BOEING

PRICES SUBJECT TO CHANGE

(NASA-CR-114489) THEORY/TEST CORRELATION
 OF HELICOPTER ROTOR BLADE ELEMENT
 AIRLOADS IN THE BLADE STALL REGIME C.J.
 Bobo (Boeing Co., Philadelphia, Pa.)
 Aug. 1972 50 p (NOAD) CSCL 01B N73-13028
 G3/02 Unclas
 50361



Reproduced by
**NATIONAL TECHNICAL
 INFORMATION SERVICE**
 U.S. Department of Commerce
 Springfield VA 22151

52P

THEORY/TEST CORRELATION
OF HELICOPTER ROTOR BLADE ELEMENT AIRLOADS
IN THE BLADE STALL REGIME

BOEING DOCUMENT D210-10508-1

By

CHRISTOPHER J. BOBO

AUGUST 1972

Prepared under Contract NAS2-5473 by
THE BOEING COMPANY, VERTOL DIVISION
Boeing Center, P.O. Box 16858
Philadelphia, Pennsylvania 19142

For

U.S. ARMY AIR MOBILITY RESEARCH AND DEVELOPMENT LABORATORY,
Ames Research Center
Moffett Field, California

and

NATIONAL AERONAUTICS AND SPACE ADMINISTRATION

SUMMARY

The experimental investigation, conducted in 1970 under the auspices of the Army Air Mobility R&D Laboratory and the National Aeronautics and Space Administration, explored the mechanisms of retreating blade stall at one spanwise location on an eight-foot diameter model rotor blade. This test program provided blade airloads and motions data for a wide range of rotor operating conditions that could be used to evaluate current theoretical representations of the complex rotor environment. As part of an additional contract awarded in 1971, a theoretical study based on this test data has been completed and is described in this report. The hybrid computer uniform downwash rotor simulation used in this study combines the storage and logic capabilities of digital equipment with the versatility of analog simulations to accommodate the complex elastic blade analysis and unsteady aerodynamics of the helicopter rotor blades.

The primary difference between the analog simulation and typical digital formulations is in the number of radial integrations or updates completed in a rotor revolution. For the typical digital program, spanwise integrations are completed every 15° of azimuth, whereas, for the hybrid simulation, radial updates occur approximately every degree of azimuth.

A comparison of experimental rotor performance data with hybrid simulation results at an advance ratio of .35 indicates that the theoretical formulation adequately predicts the rotor performance below stall but underpredicts the total lifting capability of the rotor beyond lift stall. For the advance ratio of .6, the theoretical predicted performance levels match the test data over the range of available thrusts. At the lower advance ratios, however, the limitations of uniform downwash imposed by the present hybrid formulation significantly affect the performance prediction capability.

To further evaluate current theoretical representations of the complex rotor environment, a study of pertinent parameters as a function of azimuth and span was begun. Out of this study, three significant points arose.

1. In the stalled regime, the hybrid prediction of blade flapping represents a significant improvement over the digital formulations examined.

2. The present representations of the unsteady aerodynamic lift and moment in the stall regime are inadequate.
3. In spite of deficiencies in the unsteady aerodynamic representation, the trend of the predicted growth in blade root torsion agrees well with test results.

The improvement in the predicted flapping correlation over previous digital formulations is significant in that the proper location of the rotor in space is a prerequisite for adequate prediction of rotor airloads data. The improved prediction capability of the hybrid simulation is attributed to the increased number of radial updates inherent in the analog system that could significantly affect the converged solution to the equations of motion. A study has been suggested to determine the effect of update time on digital analyses.

The deficiencies in the prediction of dynamic lift and moment levels possibly results from the manner in which two-dimensional oscillating airfoil data is used in the formulation of the dynamic stall delay. Most oscillating airfoil tests achieve representative high rates of change of α by high frequency, low amplitude sinusoidal pitching motions about moderate values of α . Data presented in this report suggests that more representative large amplitude pitch oscillations would greatly affect the value of the dynamic moment coefficient and improve the prediction of blade element loads in the stall region.

To evaluate the influence of scale effects in the model rotor test results, two separate decks of two-dimensional airfoil data representing model scale and full scale Reynolds number environments were input into the hybrid simulation. The hybrid simulation, using full scale airfoil data, accurately predicted model blade loads. Using the model scale Reynolds number airfoil data, the hybrid formulation does not properly predict model blade loads. This suggests that the effective Reynolds number of the model rotor, as it affects the blade lift, is more nearly that of a full scale rotor.

A preliminary study aimed at developing dynamic design criteria for airfoils indicates that modifying airfoil stall delay characteristics for negative values of $\dot{\alpha}$ can produce overall improvements in rotor performance and airloads. Since differences in the stall characteristics for negative $\dot{\alpha}$ and

the related damping characteristics can be changed by proper choice of airfoil, the relative benefits of the high static lift capability of leading edge stall airfoils can be traded off against the benefits of the low negative damping of trailing edge stall airfoils. Airfoil studies should continue with the aim of tailoring airfoils to produce improved stall recovery behavior without seriously limiting dynamic lift capability.

TABLE OF CONTENTS

	<u>PAGE</u>
SUMMARY	2
LIST OF ILLUSTRATIONS	6
LIST OF SYMBOLS	8
INTRODUCTION	9
HYBRID STUDY	10
THEORY/TEST COMPARISON	13
CONCLUSIONS	48
REFERENCES	49

LIST OF ILLUSTRATIONS

<u>Figure</u>		<u>Page</u>
1	Hybrid Rotor Airloads and Performance Analysis.....	11
2	Theory/Test Lift Stall Correlation, $\mu = .35$	14
3	Theory/Test Propulsive Force Correlation, $\mu = .35$	15
4	Theory/Test Lift Stall Comparison, $\mu = .6$, $\mu = .15$	16
5	Improved Flapping Prediction Capability of Hybrid Simulation.....	18
6	Normal Force Prediction Capability at 75% Radius...	20
7	Pitching Moment Prediction Capability at 75% Radius	21
8	Airloads Prediction Capability at 75% Radius.....	22
9	Elastic Pitch Contribution to Blade Element Pitch..	23
10	Influence of Pitch Amplitude on Pitching Moment Coefficient.....	25
11	Blade Torsional Load Prediction Capability, $\mu = .35$	26
12	Analog Simulation of Blade Element Lift Stall Effects, $\mu = .15$	28
13	Analog Simulation of Blade Element Moment Stall Effects, $\mu = .15$	29
14	Analog Simulation of Blade Element Lift Stall Effects, $\mu = .35$	30
15	Analog Simulation of Blade Element Moment Stall Effects, $\mu = .35$	31
16	Analog Simulation of Blade Element Moment Stall Effects, $\mu = .35$	32

<u>Figure</u>	<u>Page</u>
17 Analog Simulation of Blade Element Lift Stall Effects, $\mu = .6$	33
18 Analog Simulation of Blade Element Moment Stall Effects, $\mu = .6$	34
19 Rotor Stalled Regions at $\mu = .15$	35
20 Rotor Stalled Regions at $\mu = .35$	36
21 Rotor Stalled Regions at $\mu = .6$	37
22 Effect of Reduced Stall Hysteresis on Damping Characteristics at 50% Radius.....	39
23 Effect of Reduced Stall Hysteresis on Damping Characteristics at 75% Radius.....	40
24 Influence of Variations in Dynamic Stall Recovery at 50% Radius.....	41
25 Influence of Variations in Dynamic Stall Recovery at 75% Radius.....	42
26 Contributions of Unsteady Aerodynamics and Three Dimensional Effects at $\mu = .35$	44
27 Contributions of Unsteady Aerodynamics and Three Dimensional Effects at $\mu = .35$	45
28 Contributions of Unsteady Aerodynamics and Three Dimensional Effects at $\mu = .35$	46
29 Contributions of Unsteady Aerodynamics and Three Dimensional Effects at $\mu = .6$	47

LIST OF SYMBOLS

<u>SYMBOL</u>	<u>DESCRIPTION</u>	<u>UNITS</u>
c	Blade Chord	Feet
CM	Blade Element Pitching Moment Coefficient ~ M/qc^2	N.D.
CN	Blade Element Normal Force Coefficient ~ N/qc	N.D.
C_T/σ	Rotor Thrust Coefficient ~ $THRUST/\rho AV_T^2 \sigma$	N.D.
C_L/σ	Rotor Lift Coefficient ~ $LIFT/\rho AV_T^2 \sigma$	N.D.
q	Dynamic Pressure $1/2 \rho v_{LOCAL}^2$	lb/ft ²
RN	Reynolds Number Based on Chord	N.D.
V	Free Stream Velocity	Ft./Sec.
V _{TIP}	Rotor Tip Speed	Ft./Sec.
μ	Advance Ratio ~ V/V_{TIP}	N.D.
α	Blade Element Angle of Attack	Degrees
α_{CA}	Control Axis Angle of Attack	Degrees
α_S	Rotor Shaft Angle	Degrees
$\theta_{.75}$	Collective Pitch at 75% Radius	Degrees
θ_E	Pitch Angle Due to Blade Elasticity	Degrees
ψ	Blade Azimuth Angle	Degrees

INTRODUCTION

Helicopter forward speed and rotor design requirements have been dictated by limitations imposed by the effects of rotor blade stall. Thus, a better understanding of the stall phenomenon and a prediction capability representative of the complex rotor environment is imperative to the design of next generation helicopters. For many years, computer simulations of the helicopter rotor have not accurately predicted rotor performance or airloads above stall since they lacked proper dynamic stall characteristics and a proper representation of the three-dimensional environment of the rotor.

In 1969, Harris, et al, empirically combined the airload characteristics associated with yawed flow and of a two-dimensional airfoil oscillating in pitch, and generated an advanced rotor analysis method. These effects, when integrated over the rotor disc improved the rotor performance prediction capability, but no assessment of the capability of predicting local blade element airloads could be made without suitable test data for comparison. To provide such data, The Boeing Company, under contract to NASA, investigated the effects of stall on a rotor blade element in a three-dimensional rotating environment. The resulting model rotor test program provided blade element airloads and local boundary layer flow characteristics at the three-quarter blade radius position for a wide range of rotor operating conditions. A description of this test program and a summary of test results is given in Reference 1. The emphasis of this referenced report was primarily on test results and provided only a limited study of theory/test correlation. Therefore, an additional contract was awarded in 1971 to provide for final reduction and presentation of test data, and for a more detailed theoretical study. An informal data report containing final test data has been completed and may be obtained from the program technical monitor, W.J. McCroskey. The theoretical study, completed on the Vertol Hybrid Computer System, and the theory test comparison are the subjects of this report.

HYBRID STUDY

In the first quarter of 1972, a theoretical study was undertaken to investigate the blade loads and motions associated with a three-bladed articulated rotor operating in the blade stall regime. Data points were chosen to match test conditions recorded in the 1970 eight foot pressure blade wind tunnel test program BVWT 054.

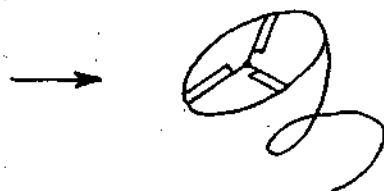
The hybrid simulation used in this theoretical study is a combination of analog and digital capabilities in that the airfoil characteristics and blade structural mode shapes are supplied to the analog equipment by a special purpose digital computer acting as a function generator. In addition, the logic and switching circuits required for the multiple integrations of this problem are provided by digital components. A description of the hybrid simulation is given in Figure 1.

The formulation of the analog analysis is one of the uniform downwash with three blade flapping modes and two blade torsion modes. The representations of unsteady aerodynamics and sweep effects are essentially the same as used in Vertol digital programs and as developed in Reference 2. The aerodynamic loads, and flapping and torsional motions resulting from these loads, are computed as they act radially along the blade. These blade loads are transferred to the appropriate coordinate system and doubly integrated to produce total rotor forces. A detailed description of the analog formulation and its capabilities is given in Reference 3.

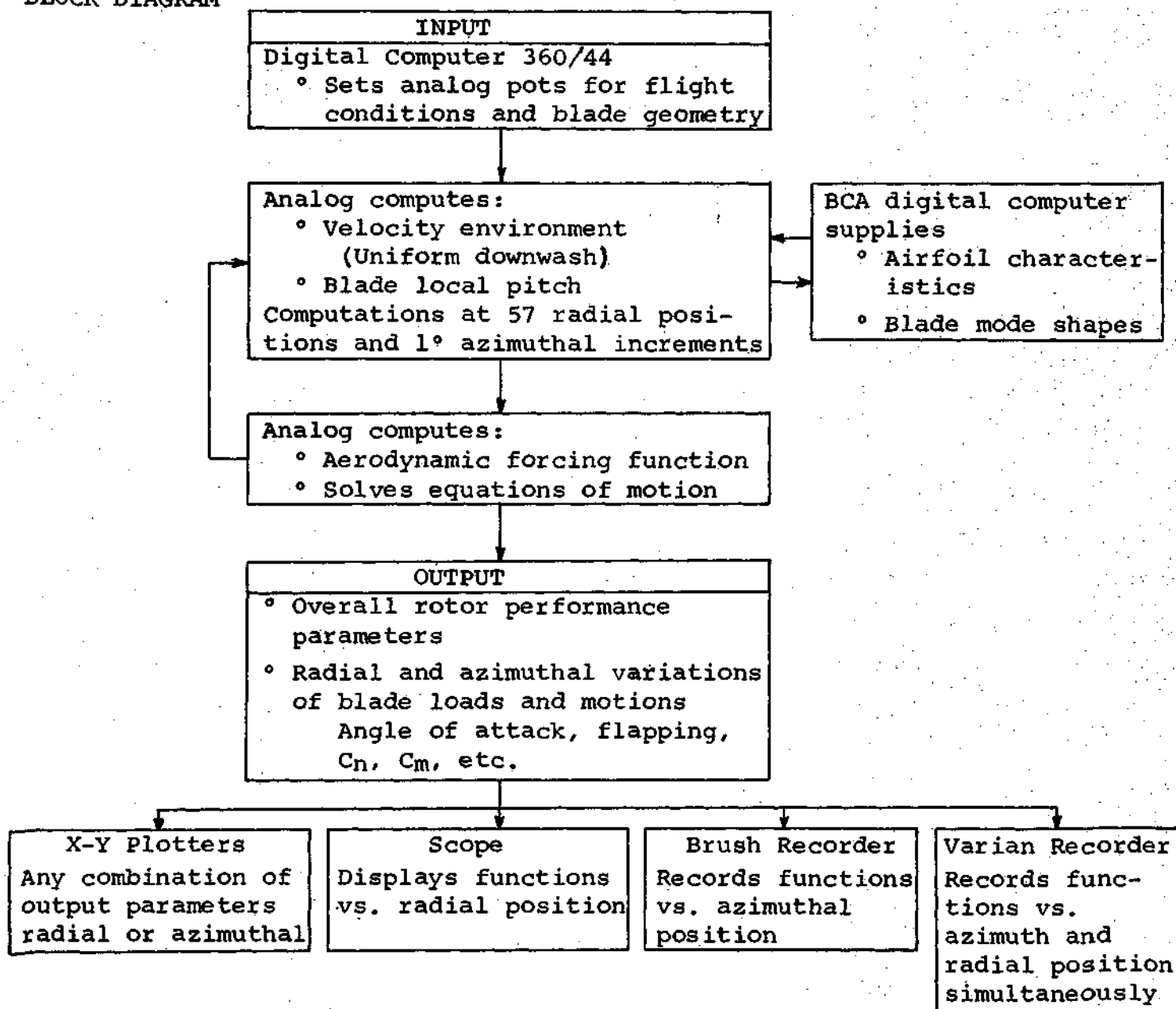
In the analog representation, the theoretical equations are transformed so that time is used to represent the azimuthal rotation of the blade as well as the radial sweep. The azimuthal integration, however, proceeds much more slowly than the radial integration. One radial integration is completed within one degree of azimuth rotation. The airloads and motions computed during this radial sweep are held and used in the azimuthal integrations until the following radial sweep. The major difference, therefore, between this hybrid simulation and standard digital programs is in the number of radial updates per rotor revolution. For typical digital programs, the spanwise integrations are completed every 15° of azimuth, and, for the hybrid simulation, radial updates occur approximately every degree of azimuth. The significance of the increased number of updates is evident when considering the formulation with higher harmonics. Since many cycles are completed for

HYBRID ROTOR AIRLOADS AND PERFORMANCE ANALYSIS

MODEL



BLOCK DIAGRAM



Basic Features

1. Visual output of results
2. Short run time
3. On-line modified formulation
4. Simplified parametric studies
5. Adaptable to a variety of rotor types - Articulated, teetering, and rigid rotors
6. Three flap modes, two torsion modes
7. Provision for coupled modes
8. Contains yawed flow and unsteady aerodynamics

each rotor revolution, increments smaller than the standard digital 15° increment are required to provide adequate representation of these higher harmonics. Such an increase in the number of radial updates for the digital computer would greatly affect the computation time and thereby the cost.

THEORY/TEST COMPARISON

Before a detailed study of the blade element airloads was begun, an assessment of the hybrid simulation capability of predicting overall rotor performance was made. The data points for this study were chosen to match test conditions recorded during the 1970 eight foot pressure blade wind tunnel test, BVWT 054. These data points included both stalled and unstalled conditions at advance ratios of .15, .35 and .6. Input parameters for the hybrid study were based on model rotor structural properties and test program control positions. At a given advance ratio, collective pitch was set to match a given test thrust and then shaft angle was varied to produce a thrust sweep. A comparison of theory and test thrust sweeps is given in Figure 2 for an advance ratio of .35. The theory indicates good agreement with test up to lift stall, but underpredicts total rotor lift beyond lift stall. This difference in rotor lift level above lift stall is evident in the curves of normal force coefficient versus azimuth which are discussed below. The additional data shown in Figure 2 represents results from a similar rotor tested under the same conditions in the University of Maryland Wind Tunnel except for the difference in collective pitch. The similarity in the trends of this test data and the theory leads to more confidence in the capability of predicting rotor performance. The comparison of theoretical and test propulsive force data in Figure 3 indicates fairly good agreement considering the magnitude of the hub tare correction applied to the test data and the trend similar to the UMWT 516 test data. Curves of BVWT 054 test data are shown with and without hub tares to emphasize the size of the hub tare correction.

Similar theory/test comparisons of rotor lift versus shaft angle at advance ratios of .6 and .15 are shown in Figure 4. At $\mu = .6$, the theory/test correlation is very good for the two different collective curves. For the lower advance ratio, a significant difference in the rotor lift curve slopes of the theory and test data is noted. This difference may be related to the significant nonuniformity in induced velocity along the longitudinal axis of the rotor as described by Harris in Reference 4.

In this reference, the existence of the wake nonuniformity is indicated by large values of lateral flapping produced at low advance ratios. The effect of this nonuniform downwash on rotor performance is minimized at large negative control axis

THEORY/TEST LIFT STALL
CORRELATION

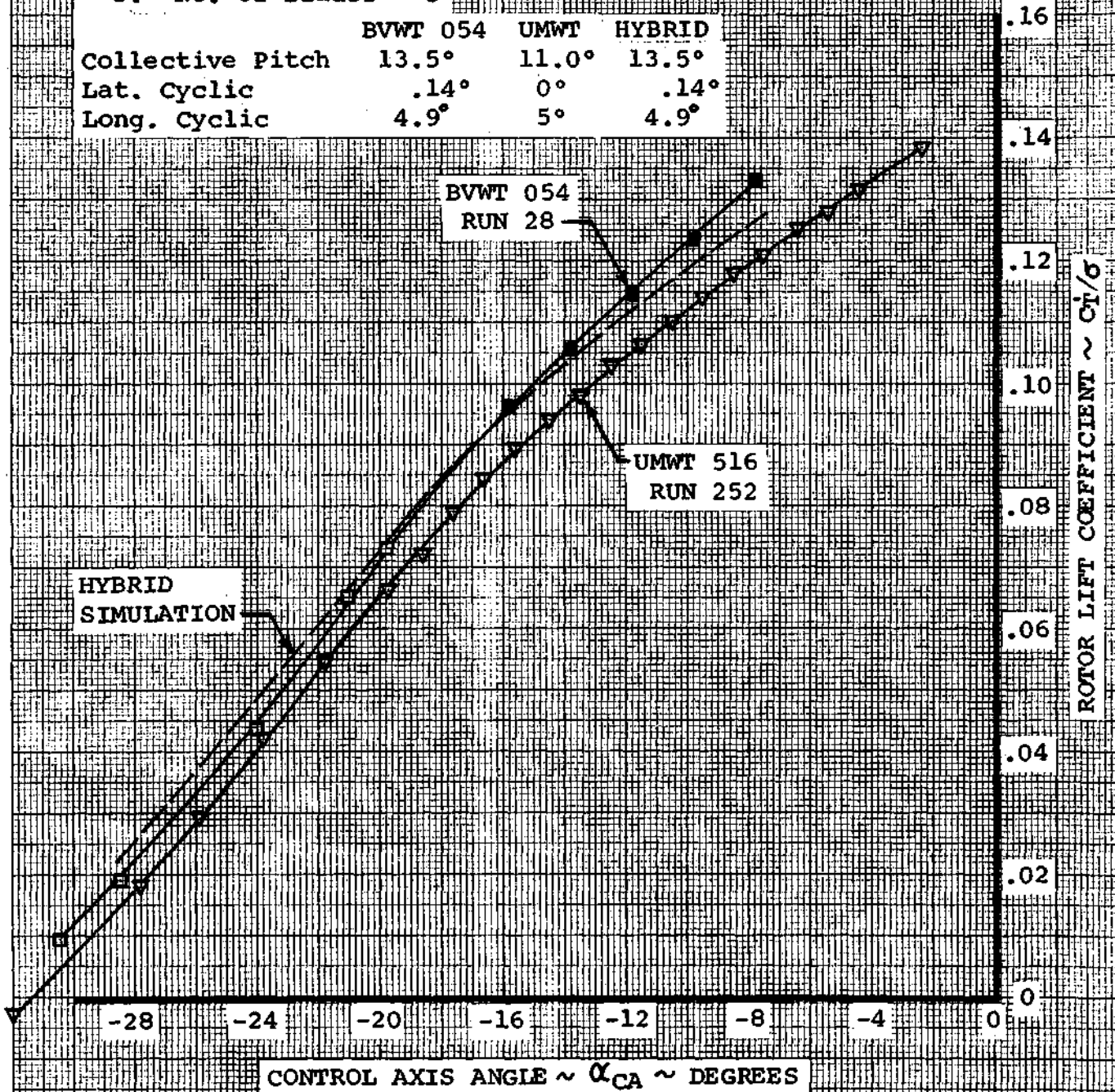
$\mu = .35$

Notes:

1. VTIP = 500 FPS
2. Radius = 4 Ft.
3. No. of Blades = 3

SOLID SYMBOLS INDICATE
STALLED BVWT 054 CONDITIONS

	BVWT 054	UMWT	HYBRID
Collective Pitch	13.5°	11.0°	13.5°
Lat. Cyclic	.14°	0°	.14°
Long. Cyclic	4.9°	5°	4.9°



EUGENE DIETZGEN CO.
MADE IN U. S. A.

NO. 340R-MP DIETZGEN GRAPH PAPER
MILLIMETER

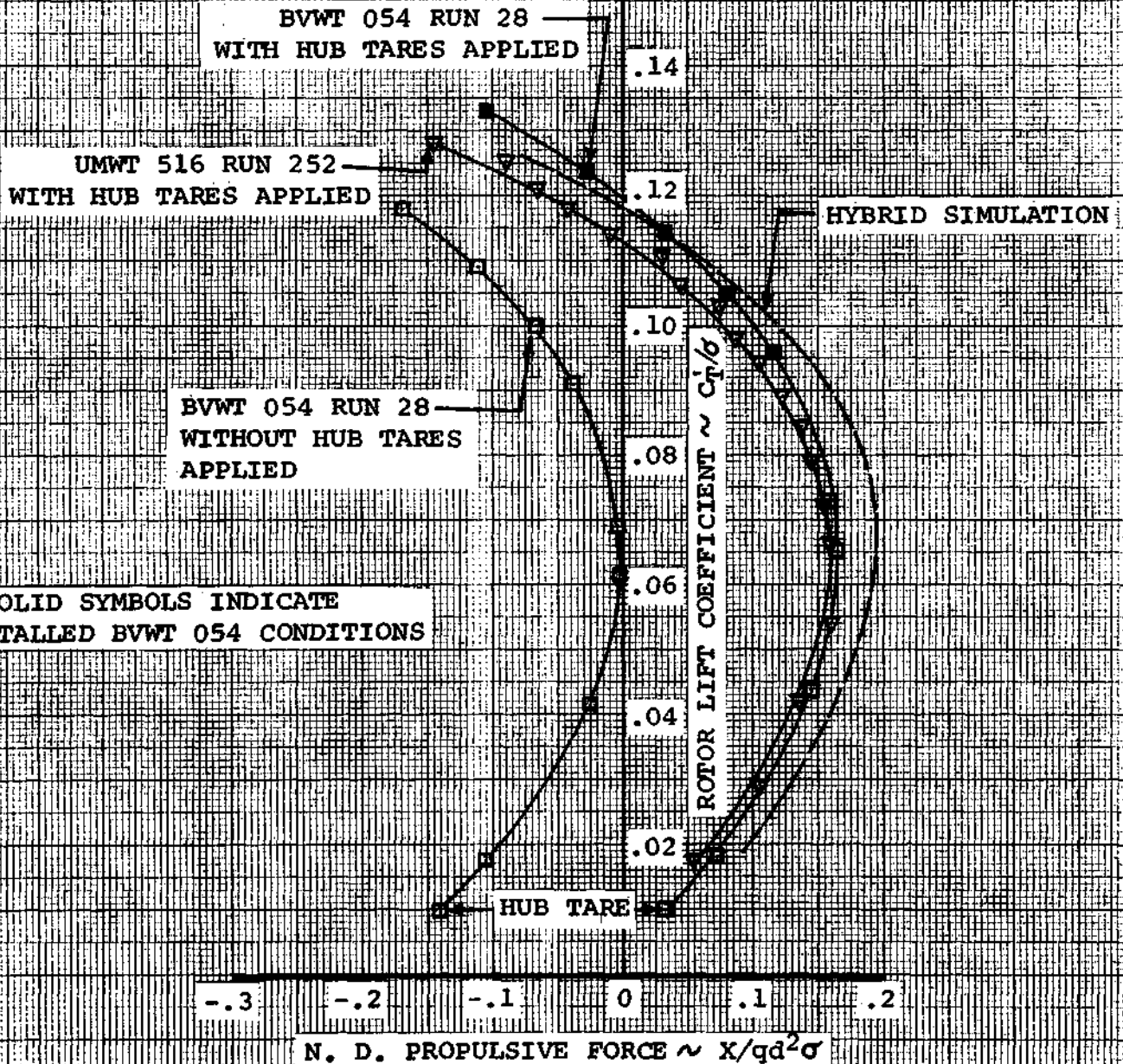
**THEORY/TEST PROPULSIVE
FORCE CORRELATION**

$\mu = .35$

Notes:

1. $V_{TIP} = 500$ FPS
2. Radius = 4 Ft.
3. No. of Blades = 3

	BVWT 054	UMWT	HYBRID
Collective Pitch	13.5°	11.0°	13.5°
Lat. Cyclic	.14°	0°	.14°
Long. Cyclic	4.9°	5°	4.9°



EUGENE DIETZGEN CO.
MADE IN U. S. A.

NO. 340R-MP DIETZGEN GRAPH PAPER
MILLIMETER

THEORY/TEST LIFT STALL COMPARISON

$\mu = .6$

Notes:

VTIP = 400 FPS
Lat. Cyclic = $.14^\circ$
Long. Cyclic = 8.72°

HYBRID
SIMULATION

BVWT 054
RUN 31
 $\Theta_{.75} = 8.5^\circ$

ROTOR LIFT
COEFFICIENT $\sim C_t/\sigma$

HYBRID
SIMULATION

BVWT 054
RUN 31
 $\Theta_{.75} = 3.4^\circ$

-8 -6 -4 -2 0 2 4

CONTROL AXIS ANGLE $\sim \alpha_{CA}$

$\mu = .15$

Notes:

VTIP = 250 FPS
Lat. Cyclic = $.20^\circ$
Long. Cyclic = 4.88°
 $\Theta_{.75} = 11.5^\circ$

HYBRID SIMULATION

BVWT 054
RUN 18

ROTOR LIFT COEFFICIENT $\sim C_t/\sigma$

-50 -40 -30 -20 -10 0

CONTROL AXIS ANGLE $\sim \alpha_{CA} \sim \text{DEGREES}$

angles (small wake skew angles). However, as the control axis angles are increased (increasing wake skew angles), the non-uniform downwash tends to reduce the lift on the aft portion of the rotor disc and produce an overall reduction in the total rotor lift curve slope. The comparison of the uniform downwash theoretical solution with the nonuniform downwash test data shown in Figure 4 clearly illustrates such a change in overall rotor lift curve slope.

Encouraged by the reasonable agreement between the hybrid simulation and test overall rotor performance, at advance ratios of .35 and .6, a study of predicted blade root flapping was made to further evaluate the applicability of the hybrid simulation. In typical digital formulations of the rotor environment, the inability to predict blade flapping has been a serious shortcoming. Without proper representation of flapping, a theoretical formulation does not properly locate the rotor in space and, therefore, cannot provide the required velocity or angle of attack environment. Any attempted study of the resulting blade loads could prove to be misleading.

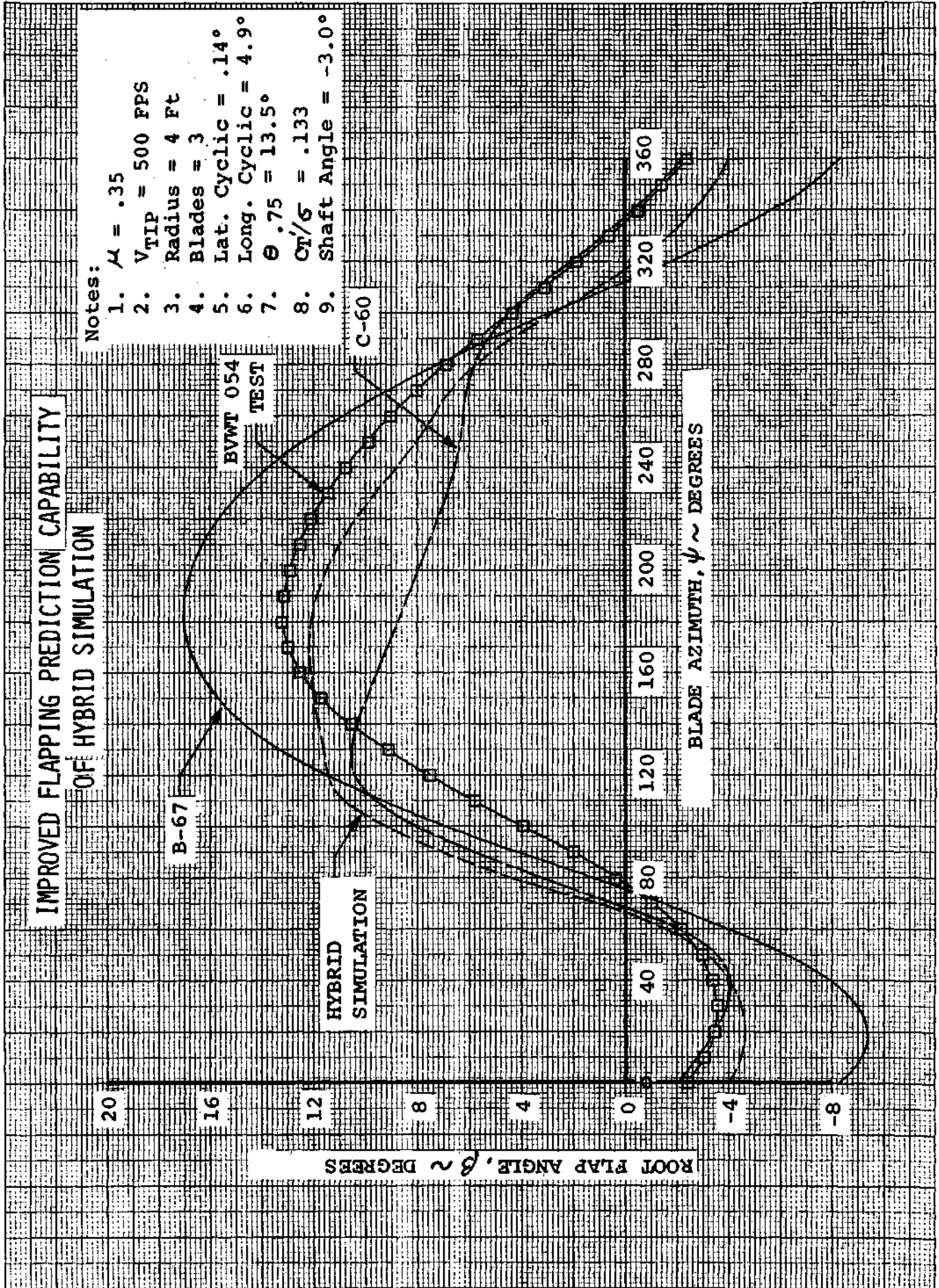
Figure 5 provides a comparison of the hybrid root flapping prediction with the results of two current digital formulations (Vertol Programs B-67 and C-60) at an advance ratio of .35. The B-67 digital program is a rotor airload and performance analysis representing the blade by a series of blade segments producing a multi-filament near field, mid field, and far field vortex pattern and nonuniform induced inflow. The modal analysis utilizes two flapping modes and one elastic torsion mode, without flap-pitch coupling. Further description of this program is provided in Reference 5. The Vertol C-60 digital program employs a lumped mass model of the rotor providing results up to ten harmonics. The flap and pitch motions of the blade are coupled and the hub and lower controls are included in the analysis. The present wake representation includes only tip and root vortices. The C-60 data presented in this report was based on a uniform downwash program option described in Reference 6. The unsteady aerodynamics formulations of the Hybrid, B-67, and C-60 simulation are essentially the same. The comparison presented in Figure 5 clearly points out the shortcomings of present digital formulation in positioning the rotor in space. The hybrid results, although still short of complete agreement, provide the best correlation to date with test flapping data.

EUGENE DIETZGEN CO.
MADE IN U. S. A.

NO. 340R-MP DIETZGEN GRAPH PAPER
MILLIMETER

IMPROVED FLAPPING PREDICTION CAPABILITY
OF HYBRID SIMULATION

- Notes:
1. $\mu = .35$
 2. $V_{TIP} = 500$ FPS
 3. Radius = 4 Ft
 4. Blades = 3
 5. Lat. Cyclic = $.14^\circ$
 6. Long. Cyclic = 4.9°
 7. $\theta = .75 = 13.5^\circ$
 8. $C_T/\sigma = .133$
 9. Shaft Angle = -3.0°



Similar improvements in flapping correlation were noted for all thrust levels at the advance ratios of .35 and .6. For the lower advance ratio, $\mu = .15$, however, the hybrid solution produces no significant improvement. The differences in the predicted and test recorded thrust levels discussed above, relating to the limitations of uniform downwash, significantly affect the prediction capability at this advance ratio. It should be pointed out here that no systematic investigation was undertaken at the time of this study to improve the hybrid flapping correlation further; however, such a study could prove to be beneficial.

Since the aerodynamic formulations of the B-67, C-60 and hybrid simulations are very similar, the differences in flapping results could be attributed to the manner in which the dynamic characteristics are considered. The present digital formulations are limited in the number of radial calculations per rotor revolution to fifteen because of the run time and cost imposed by smaller increments. The increased number of radial updates inherent in the hybrid simulation (360 per revolution) could significantly affect the converged solution to the equations of motion and the proper representation of higher elastic modes. It is suggested that a study be conducted on the effects of updating time on blade loads and motions and particularly on root flapping. This could be accomplished by changing the number of radial computations performed by the B-67 digital analysis in a given rotor revolution.

A comparison of predicted blade element airloads and motions with test results obtained from the pressure blade program provides an informative overview of the theoretical capability of this hybrid program. The curves of Figures 6 through 9 provide theory/test comparison of blade element normal force coefficient, moment coefficient and blade pitch at the three-quarter radius station. The predicted levels of normal force and moment coefficient are significantly underpredicted on the retreating portion of the rotor disc. There are indications that similar shortcomings exist in other theoretical analyses, Reference 7. The theoretical formulation of the unsteady aerodynamic nature of the flow relies on a representation of the dynamic lift and moment based on oscillating airfoil test data. McCroskey points out in Reference 8 that the present computations of lift and moment overshoot are based on oscillating airfoil data which are not representative of the azimuthal variation of α exhibited by the rotor. Most oscillating airfoil studies have been conducted using high frequency, low

EUGENE DIETZGEN CO.
MADE IN U. S. A.

NO. 34DR-MP DIETZGEN GRAPH PAPER
MILLIMETER

NORMAL FORCE PREDICTION CAPABILITY

AT 75% RADIUS

BVWT 054
RUN 28 TP 12

HYBRID
SIMULATION

Notes:

1. $M = .35$
2. VTIP = 500 FPS
3. Radius = 4 Ft.
4. Blades = 3
5. Lat. Cyclic = $.14^\circ$
6. Long. Cyclic = 4.9°
7. Collective Pitch = 13.5°
8. $CT/\sigma = .133$
9. Shaft Angle = -3.0°

2.4

2.0

1.6

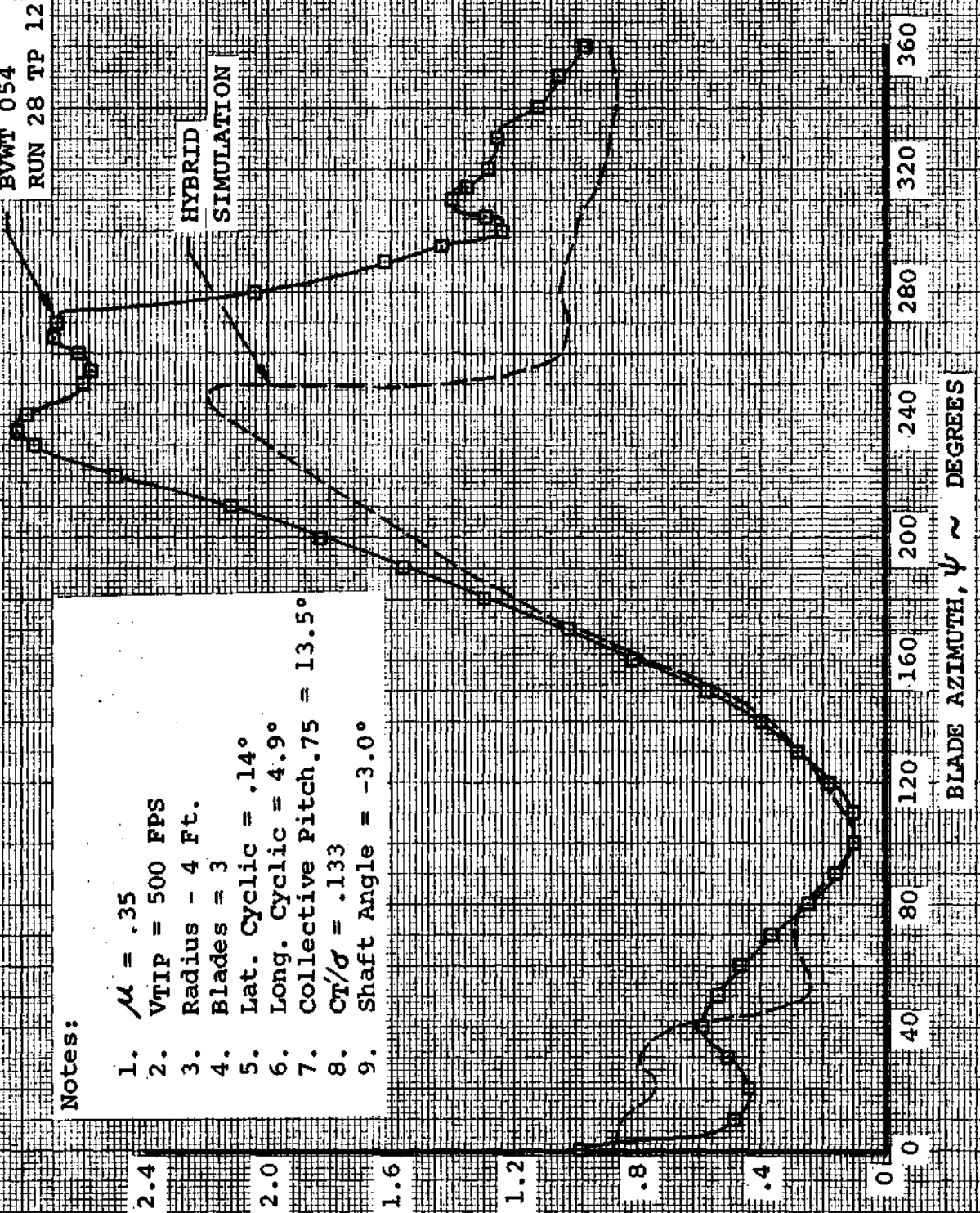
1.2

.8

.4

0

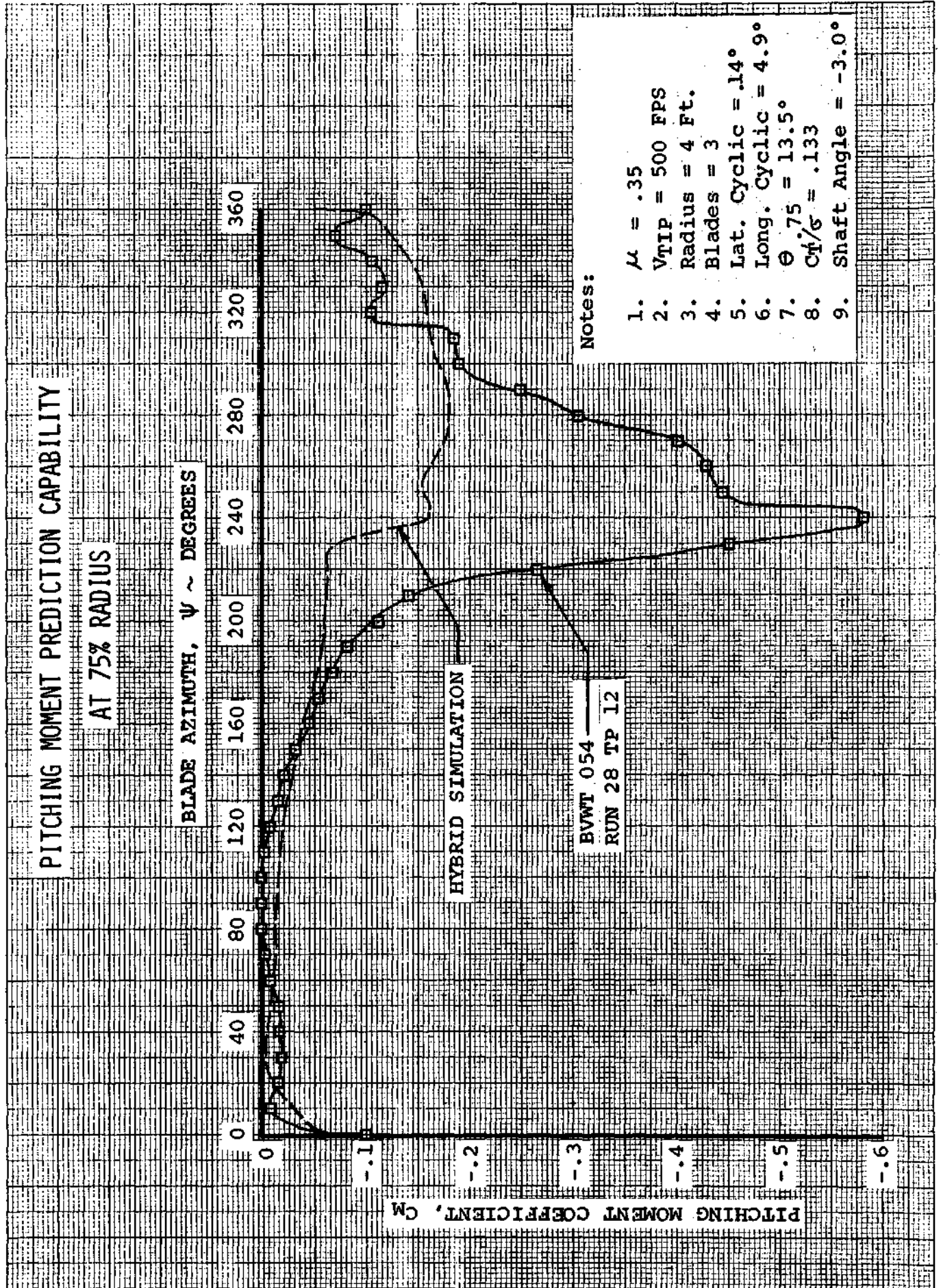
NORMAL FORCE COEFFICIENT, C_N



BLADE AZIMUTH, ψ ~ DEGREES

EUGENE DIETZEN CO.
MADE IN U. S. A.

NO. 340R-MP DIETZEN GRAPH PAPER
MILLIMETER



EUGENE DIETZGEN CO.
MADE IN U. S. A.

NO. 340R-MP DIETZGEN GRAPH PAPER
MILLIMETER

**AIRLOADS PREDICTION CAPABILITY
AT 75% RADIUS**

NORMAL FORCE COEFFICIENT, C_N

0 0.4 0.8 1.2 1.6 2.0 2.4 2.8 3.2

HYBRID
SIMULATION

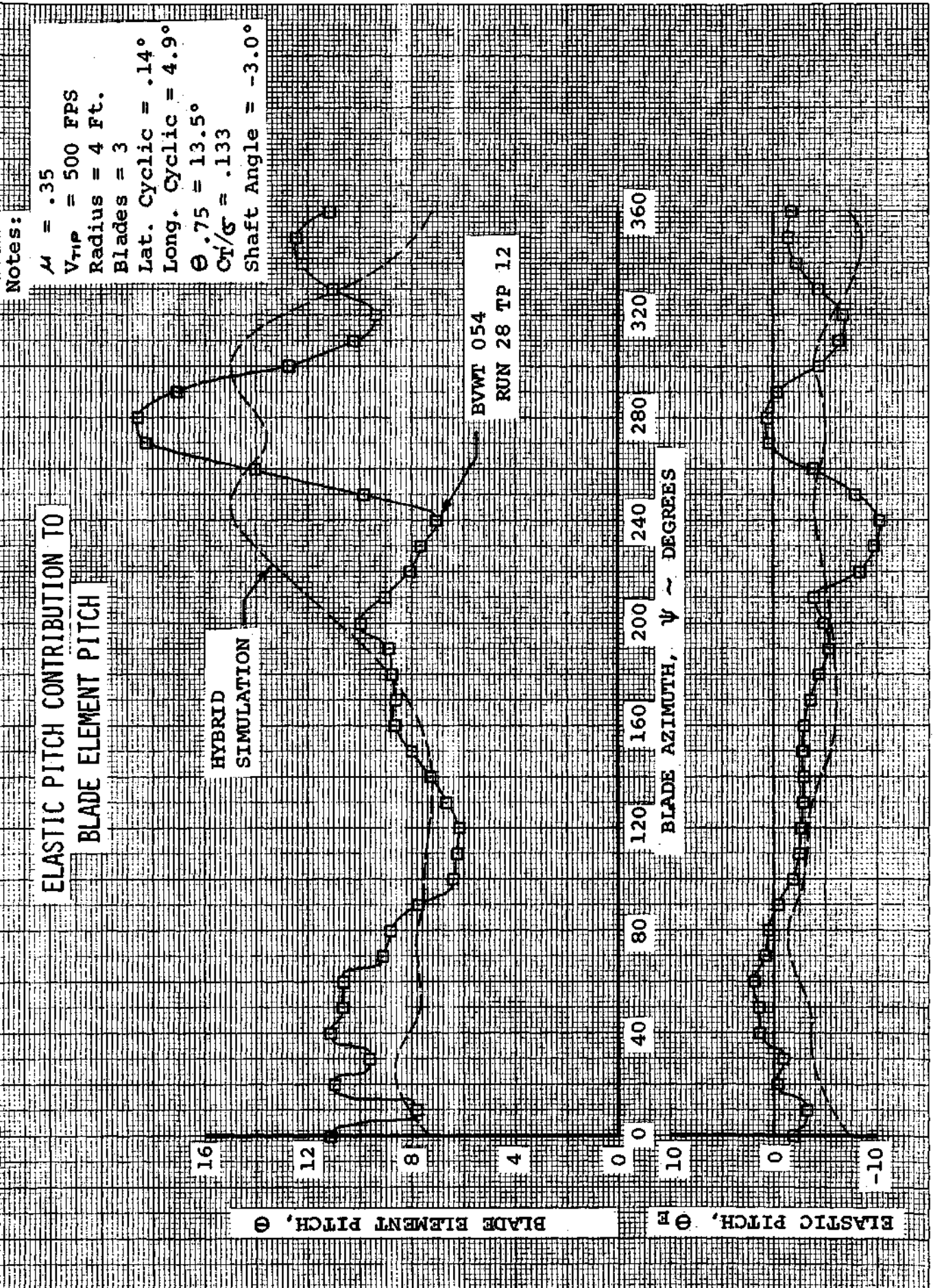
BVWT 054
RUN 28 TP 12

PITCHING MOMENT COEFFICIENT, C_M

-0.1
-0.2
-0.3
-0.4
-0.5
-0.6

Notes:

1. $\mu = .35$
2. VTIP = 500 FPS
3. Radius = 4 Ft.
4. Blades = 3
5. Lat. Cyclic = $.14^\circ$
6. Long. Cyclic = 4.9°
7. $\theta_{.75} = 13.5^\circ$
8. $CT'/_s = .133$
9. Shaft Angle = -3.0°



amplitude sinusoidal motions about small mean values of α . The angle of attack variation with azimuth for a rotor more nearly resembles a large amplitude sine wave at the fundamental rotor frequency. An investigation of available oscillating airfoil data including oscillations up to $\pm 10^\circ$ indicates that the value of dynamic moment is influenced by the amplitude of oscillation. Figure 10 presents oscillating airfoil data from Reference 9 at mean angles of 10° and 15° , illustrating a definite increase in minimum moment coefficient with increases in the amplitude of oscillation. Further study into the effects of the oscillating airfoil pitch amplitude on the theoretical unsteady aerodynamic γ function representation and the resulting effects on dynamic lift and moment should be made to improve existing theoretical models.

It is generally recognized that the moment stall indicated in Figure 7 has a significant effect on rotor control loads and in particular on the blade torsion loads. The influence of the large negative pitching moments in stall can be seen in Figure 9 since the elastic twist is linearly proportional to the blade torsion at the root of the blade. The large pitching moment generated at 240° is reflected as a nose down pitching motion of approximately 10° . With the following reduction in $-C_m$, the blade begins a rapid pitch up motion followed by several oscillatory cycles commonly termed stall flutter. Since the hybrid simulation fails to predict the large pitching moments associated with stall, the resulting blade pitching of Figure 9 does not provide a representative picture of the stall flutter motion.

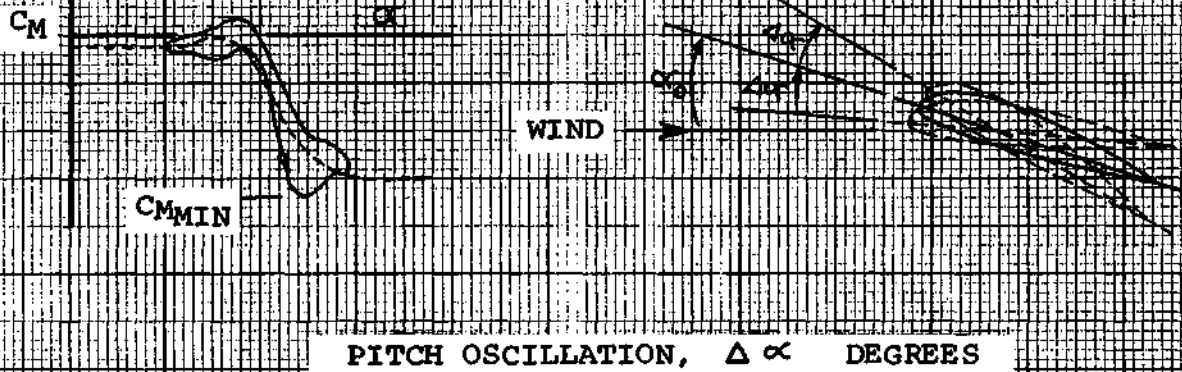
The curves of Figure 11 illustrate the growth of blade root torsion with rotor lift coefficient. The hybrid results, compared to the measured test torsion results, were obtained from the theoretical elastic twist values assuming that the majority of the elastic twist comes from the first torsional mode. The trend of the hybrid results, based on full scale Reynolds number two-dimensional airfoil data, compares well with the test data except at the high thrust levels where large portions of the rotor are stalled. The incremental differences between the two curves, below stall, could be attributed to improper representation of the two-dimensional pitching moment level. A closer look at the torsional waveforms for the thrust conditions above stall indicates that the hybrid solution does not predict the large oscillation in torsion beginning in the third quadrant. As mentioned above, these differences arise from an improper theoretical represen-

INFLUENCE OF PITCH AMPLITUDE ON PITCHING MOMENT COEFFICIENT

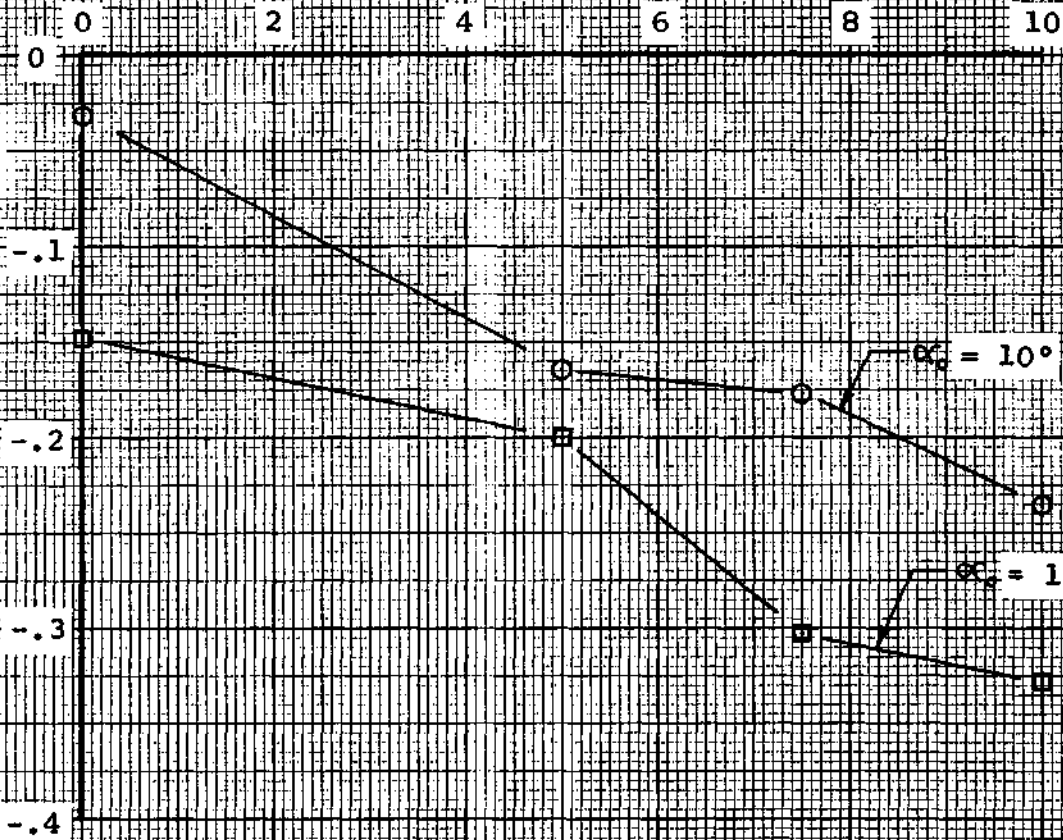
Notes:

MACH NO. = .4

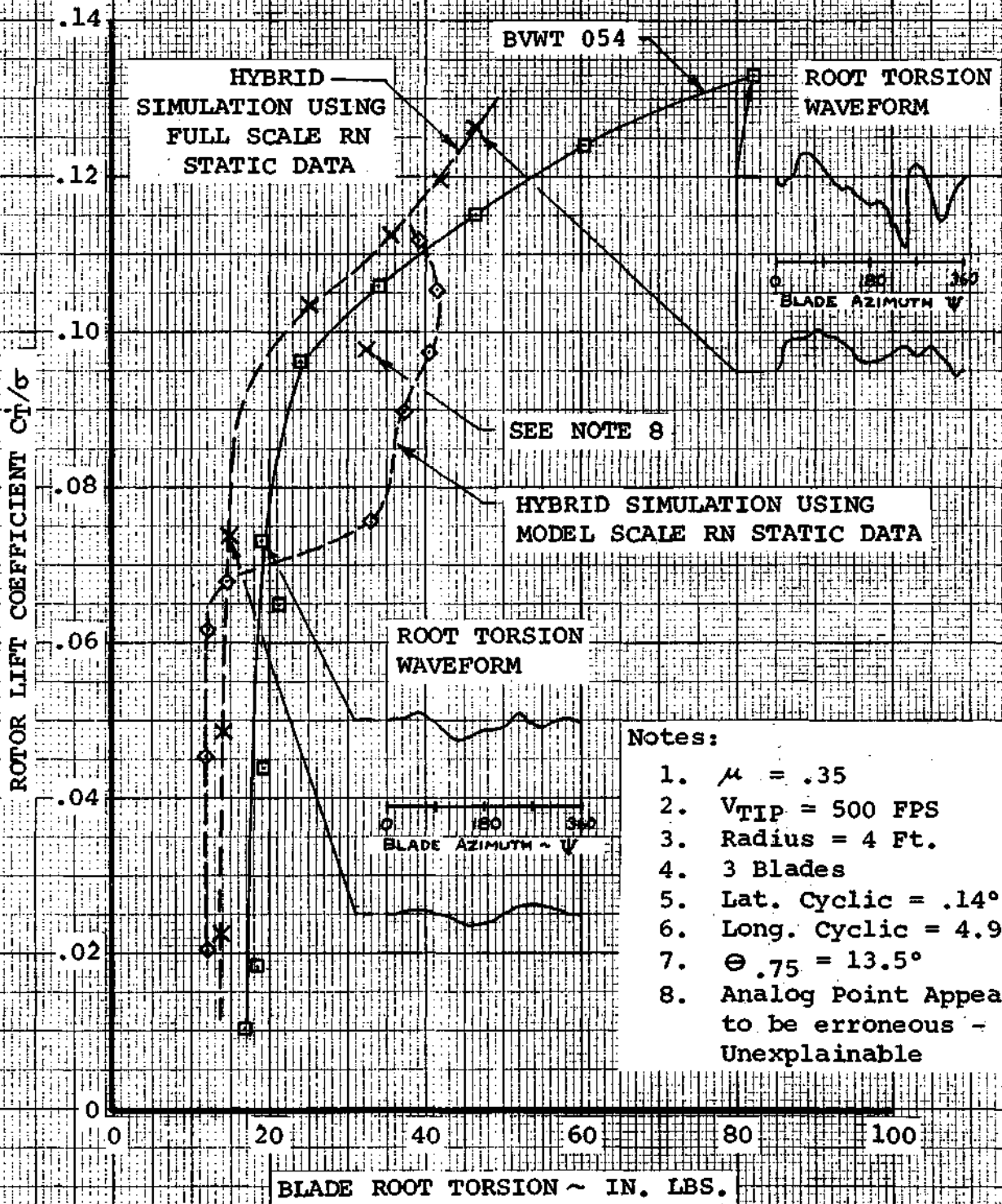
1. $K = \text{Reduced Frequency, } \pi fc/V = .06$
2. Reference: USAVLABS TR 68-89B



MAXIMUM NEGATIVE PITCHING
MOMENT COEFFICIENT, $C_{M \text{ MIN}}$



BLADE TORSIONAL LOAD PREDICTION CAPABILITY



- Notes:
1. $\mu = .35$
 2. $V_{TIP} = 500$ FPS
 3. Radius = 4 Ft.
 4. 3 Blades
 5. Lat. Cyclic = $.14^\circ$
 6. Long. Cyclic = 4.9°
 7. $\Theta .75 = 13.5^\circ$
 8. Analog Point Appears to be erroneous - Unexplainable

EUGENE DIETZGEN CO.
MADE IN U. S. A.

NO. 340R-20 DIETZGEN GRAPH PAPER
20 X 20 PER INCH

tation of the dynamic moments in the stall region. An interesting comparison is noted in Figure 11 between the curves of test data and hybrid results based on model scale Reynolds number airfoil data. The growth in blade root torsion exhibits a character altogether different from the test results. This comparison indicates, as was pointed out in Reference 1, that even though the Reynolds number on the model blades is an order-of-magnitude lower than the full-scale rotor blades, the resulting blade loads exhibit characteristics similar to full scale high Reynolds number data.

Due to the complexity of blade pressure instrumentation and limitations of data acquisition systems, rotor test programs have not recorded blade element airloads over a complete range of spanwise stations. Data from the BVWT 054 test is available only at the three-quarter radius station. Using the varied output capability of the analog system, blade element airloads were recorded as a function of blade azimuth and span for each of the three advance ratios of .15, .35 and .6. Curves of normal force coefficient and moment coefficient spanwise distributions are given in Figures 12 through 18. Data within the reverse flow region has not been included in these figures. Using this data and the results from Varion traces, which provide similar data at each azimuth location, a summary of the lift stall and moment stall distributions around the rotor disc was made. Examples of these stall areas are illustrated in Figures 19, 20 and 21. The azimuth positions for blade element lift and moment stall, as obtained from test data at the three-quarter radius, are indicated in each figure. The hybrid representation of the rotor tends to stall later and unstall earlier than the test results.

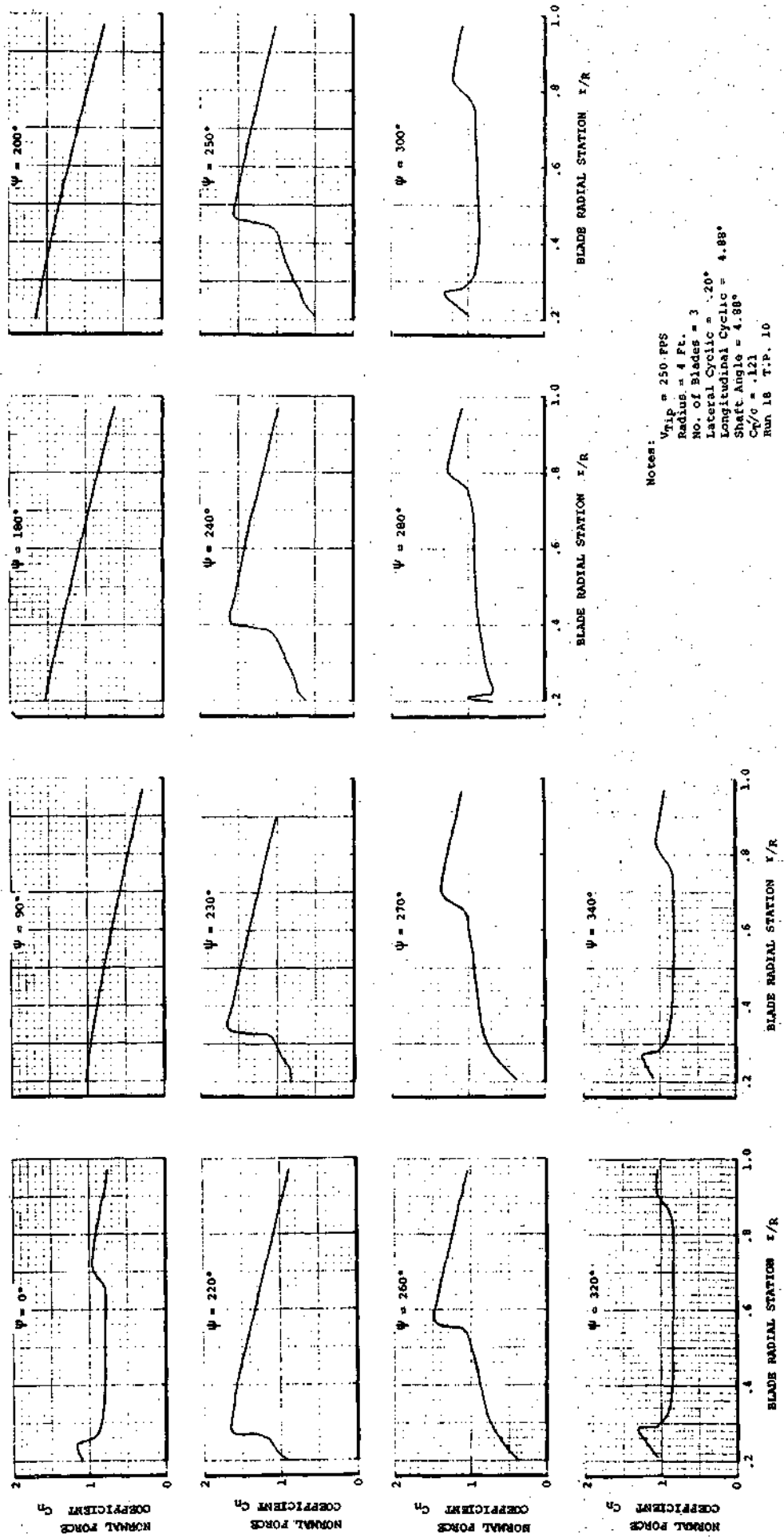
In the unsteady aerodynamic theory, the experimentally derived equation for dynamic stall delay is given as:

$$\text{Dynamic stall delay} = \gamma \sqrt{\frac{\dot{\alpha} C}{2 V}}$$

This equation is used in such a manner that as long as the time rate of change of angle of attack, $\dot{\alpha}$, remains positive and of sufficient magnitude, stall will not occur. Thus, an airfoil experiencing stall delay must stall on or before the condition of $\dot{\alpha} = 0$. This condition of $\dot{\alpha} = 0$ has been noted at the three-quarter radius location on the stall regions of Figures 19, 20 and 21. In each case, the lift stall and moment stall occur prior to the condition of $\dot{\alpha} = 0$. The magnitude

ANALOG SIMULATION OF BLADE ELEMENT LIFT STALL EFFECTS

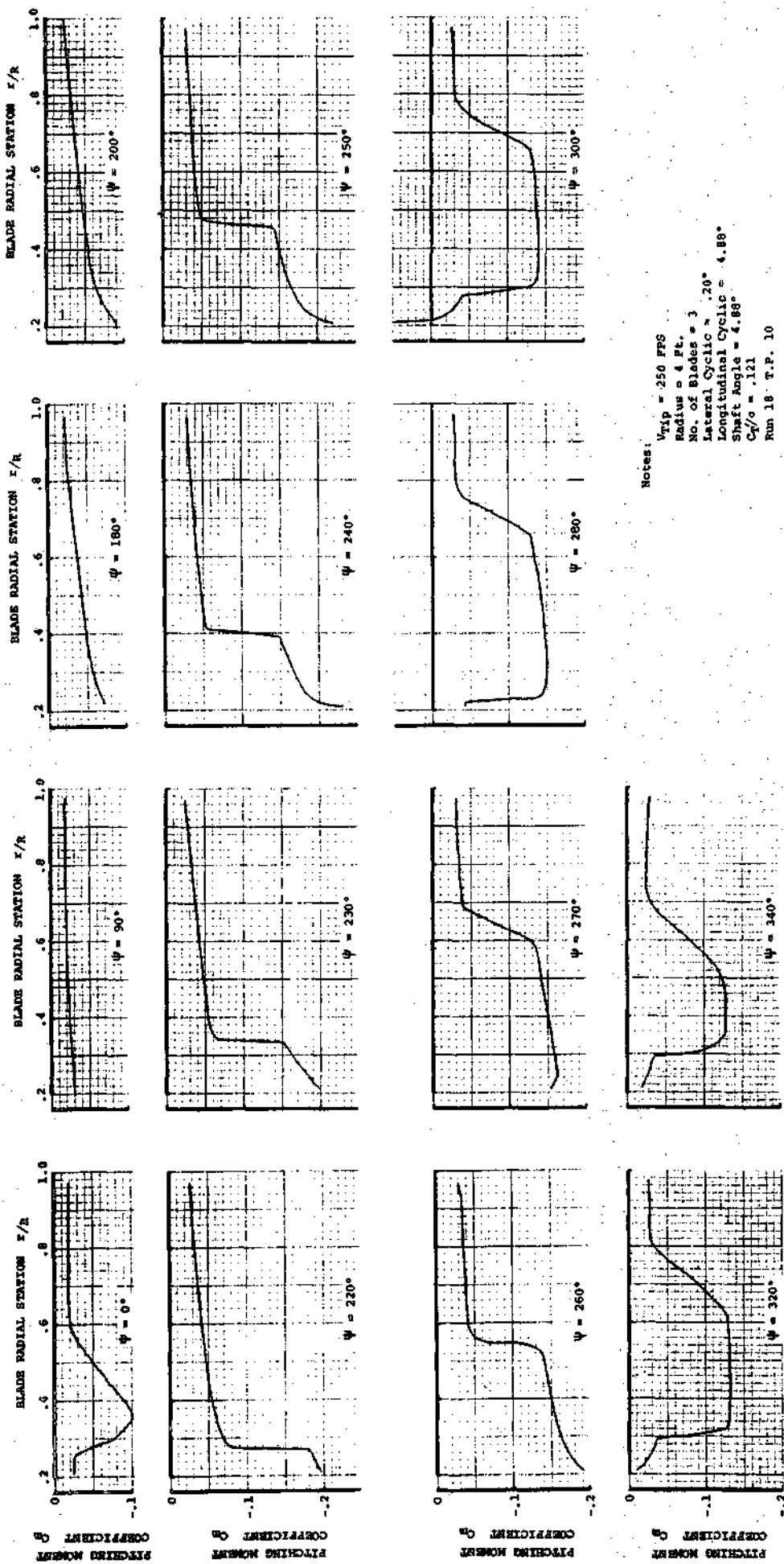
$\alpha = .15$



Notes:
 $V_{tip} = 250$ FPS
 Radius = 4 Ft.
 No. of Blades = 3
 Lateral Cyclic = .20°
 Longitudinal Cyclic = 4.88°
 Shaft Angle = 4.88°
 $C_{y/c} = .121$
 Run 18 T.P. 10

ANALOG SIMULATION OF BLADE ELEMENT MOMENT STALL EFFECTS

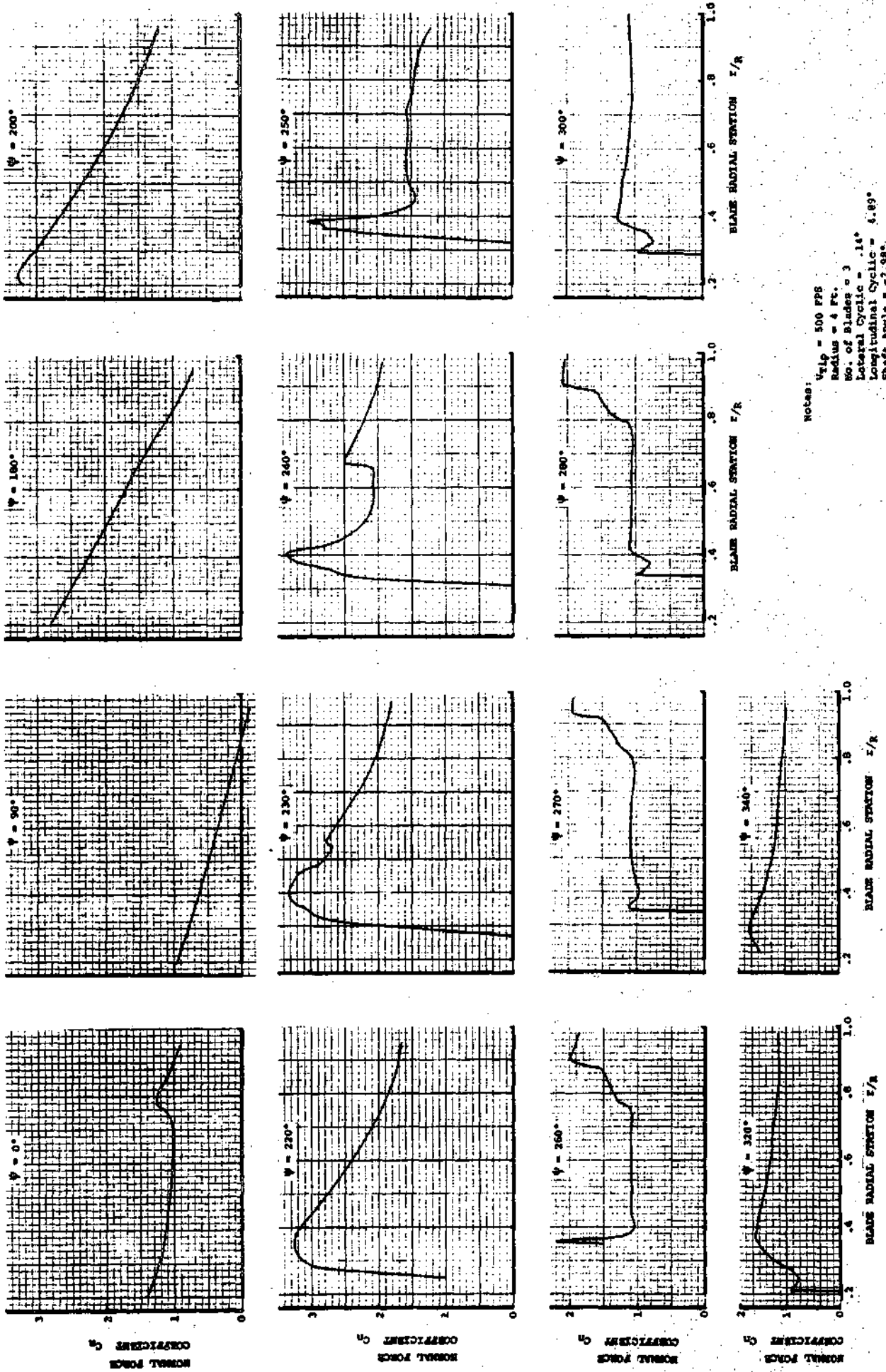
$\mu = .15$



Notes:
 Vtip = 250 FPS
 Radius = 4 Ft.
 No. of Blades = 3
 Lateral Cyclic = .20°
 Longitudinal Cyclic = 4.88°
 Shaft Angle = 4.88°
 C_p/σ = .121
 Run 18 T.P. 10

ANALOG SIMULATION OF BLADE ELEMENT LIFT STALL EFFECTS

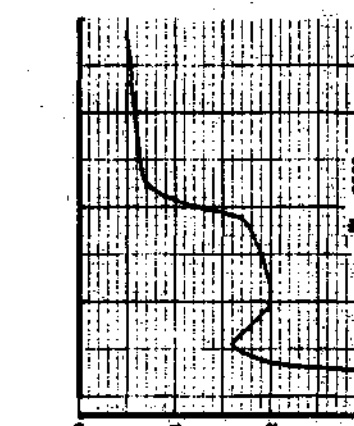
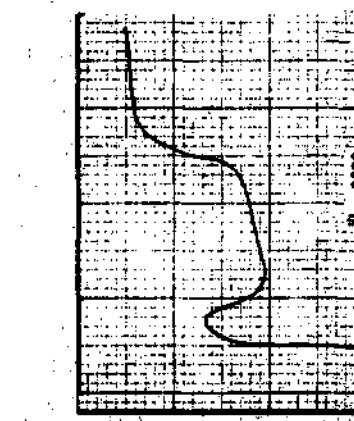
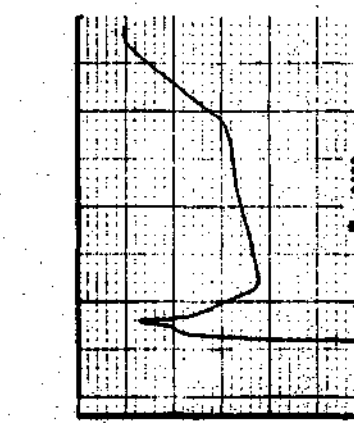
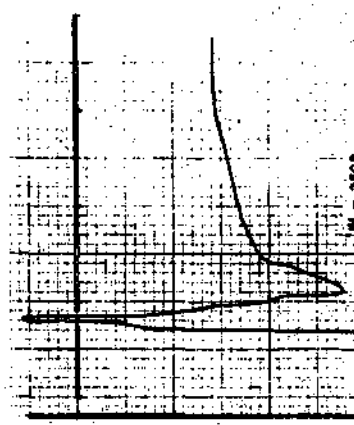
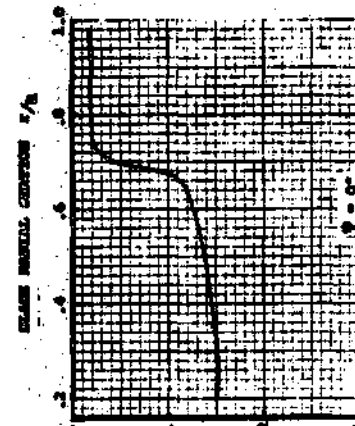
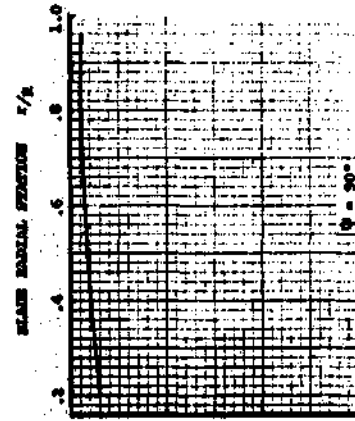
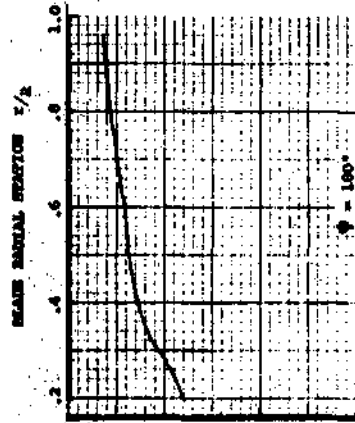
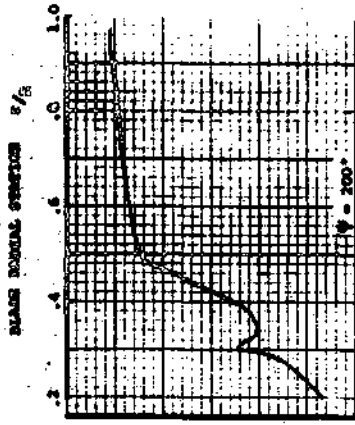
$M = .35$



Notes:
 $V_{tip} = 500$ FPS
 Radius = 4 Ft.
 No. of Blades = 3
 Lateral Cyclic = $.14^\circ$
 Longitudinal Cyclic = 4.89°
 Shaft Angle = -2.98°
 $C_T/\rho = .1133$
 Run 28 T.P. 12

ANALOG SIMULATION OF BLADE ELEMENT MOMENT STALL EFFECTS

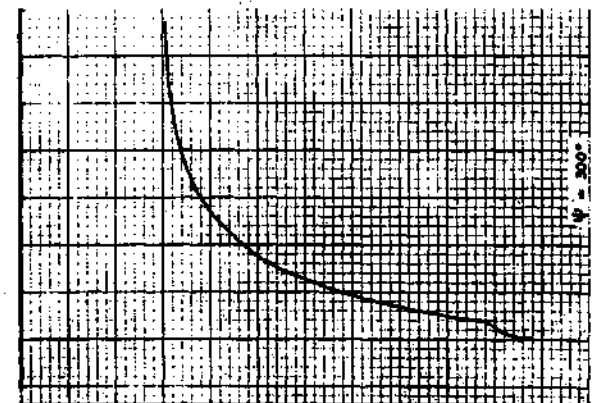
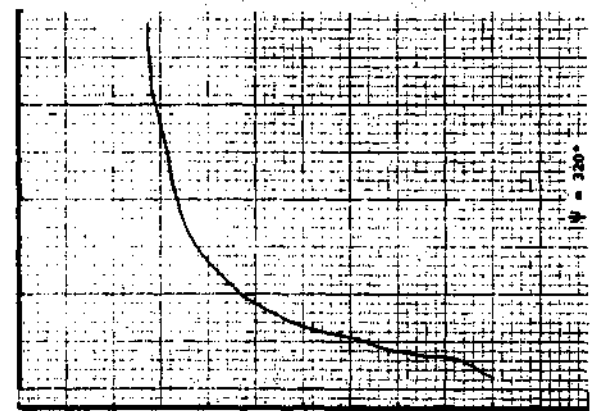
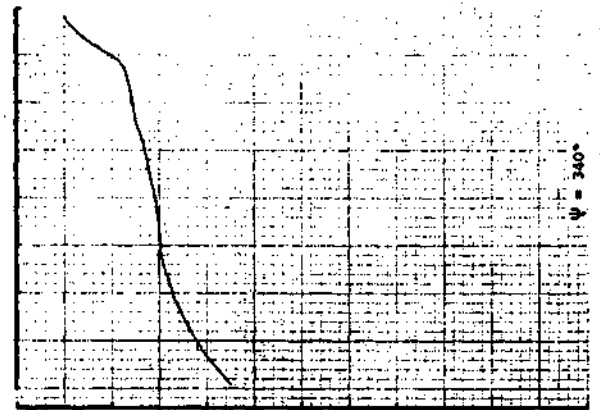
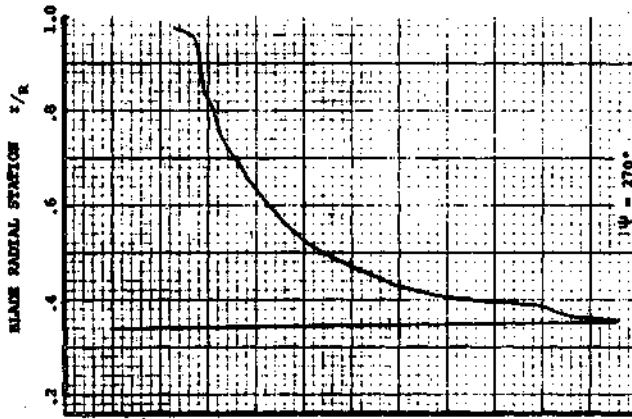
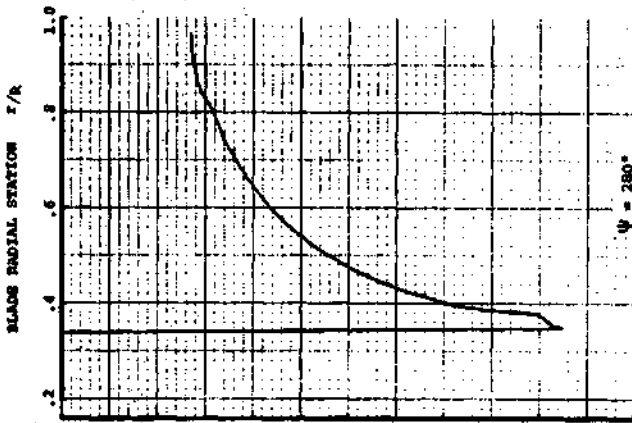
$\lambda = .35$



Recess
 Tip = 500 rps
 Radius = 4 ft.
 No. of blades = 3
 Lateral cyclic = .14°
 Longitudinal cyclic = 4.89°
 Mast angle = -2.88°
 C/L = .133
 SMO 28 S.P. 12

ANALYSIS OF BLADE ELEMENT MOMENT STALL EFFECTS

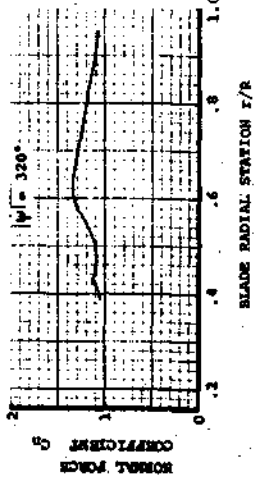
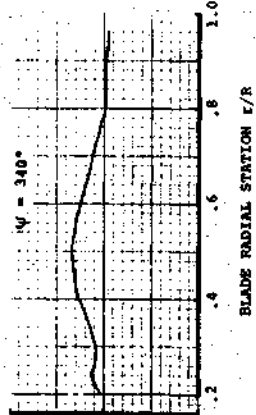
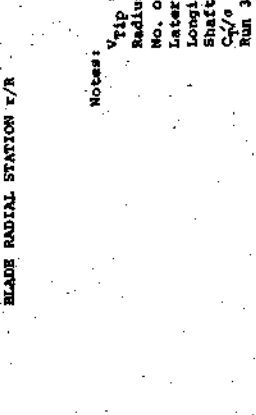
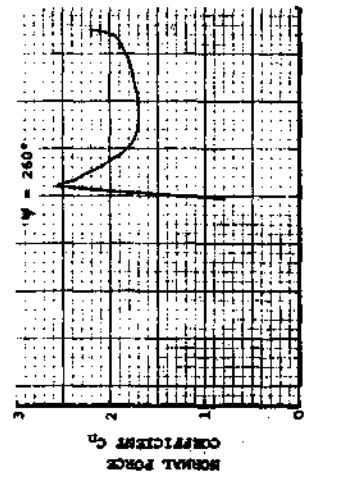
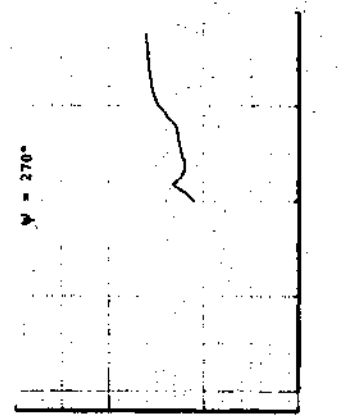
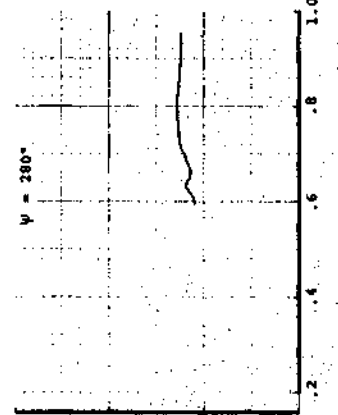
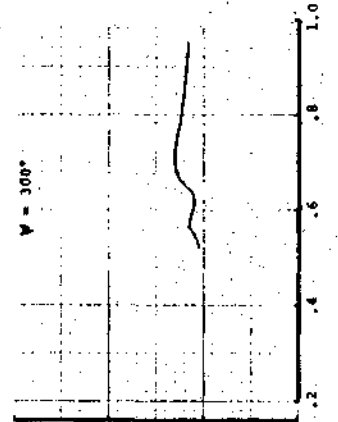
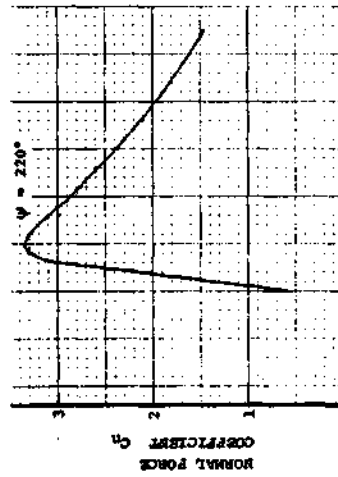
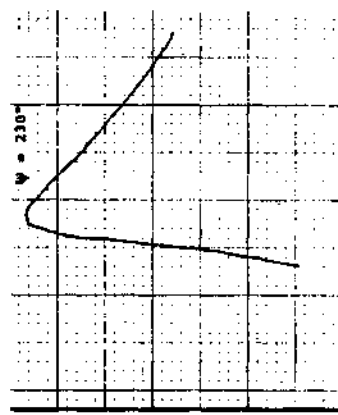
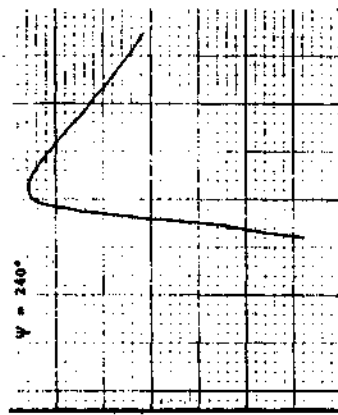
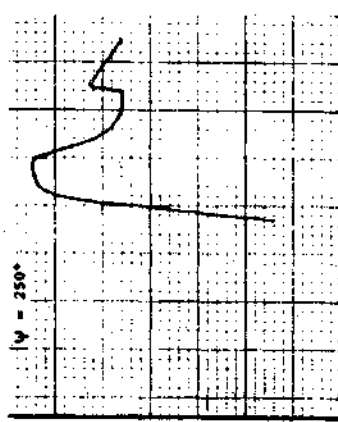
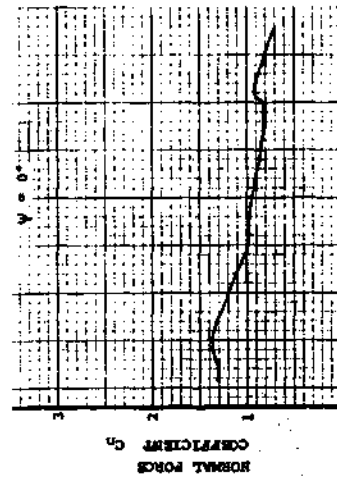
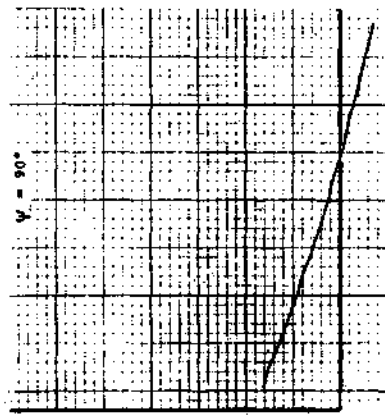
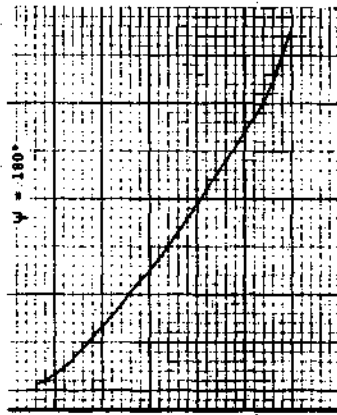
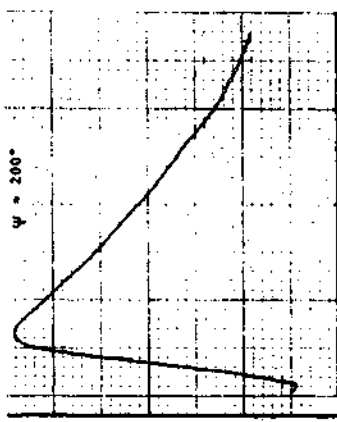
$\lambda = .35$



Notes:
 $V_{tip} = 500$ FPS
 Radius = 4 Ft.
 No. of Blades = 3
 Lateral Cyclic = .14°
 Longitudinal Cyclic = 4.88°
 Shaft Angle = -2.98°
 $C_p/a = .133$
 Run 28 T.P. 12

ANALOG SIMULATION OF BLADE ELEMENT LIFT STALL EFFECTS

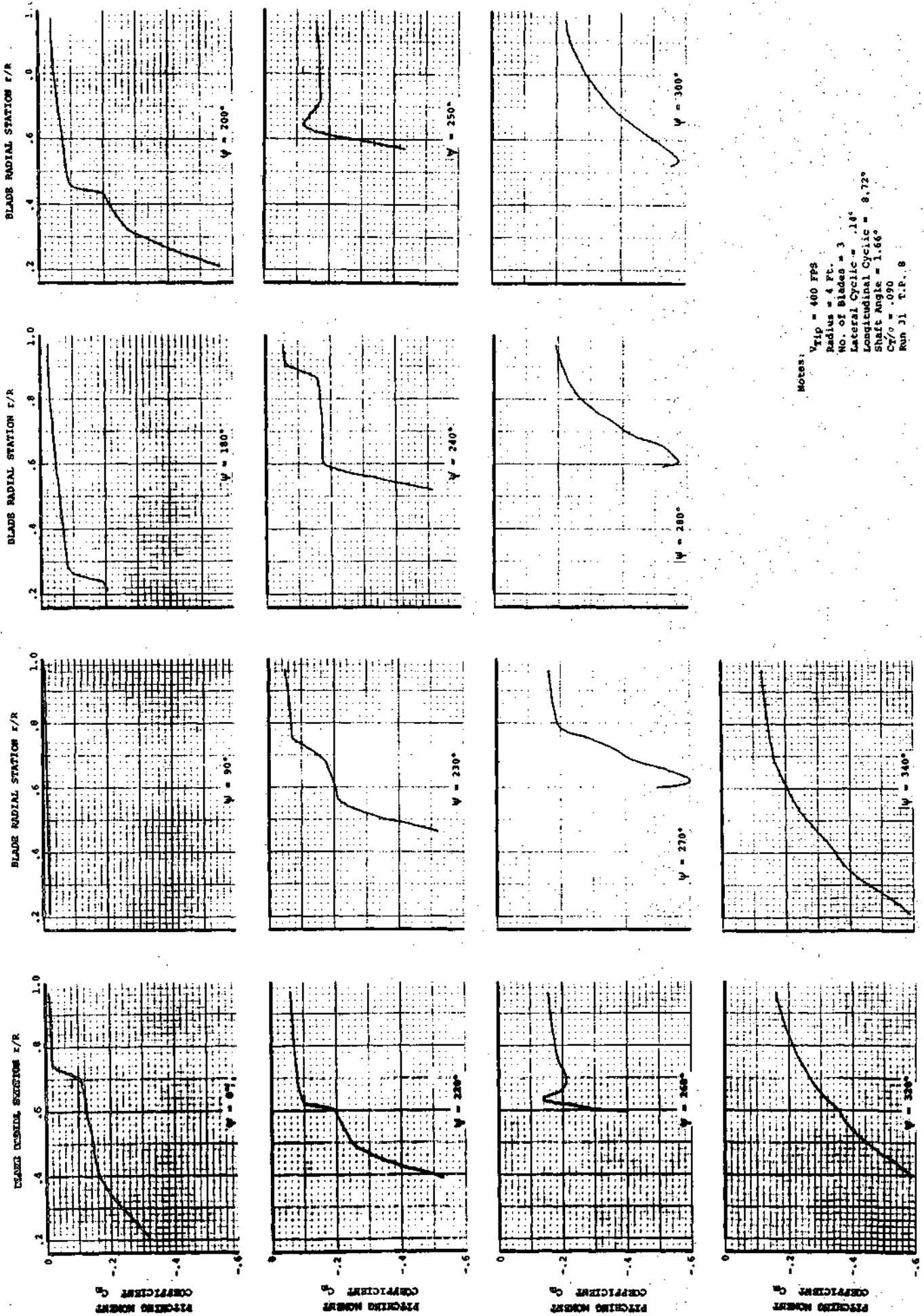
$\mu = .60$



Notes:
 $V_{tip} = 400$ FPS
 Radius = 4 Ft.
 No. of Blades = 3
 Lateral Cyclic = .14°
 Longitudinal Cyclic = 3.72°
 Shaft Angle = 1.66°
 $C_{y/c} = .090$
 Run 31 T.P. 8

ANALOG SIMULATION OF BLADE ELEMENT MOMENT STALL EFFECTS

$\lambda = .60$



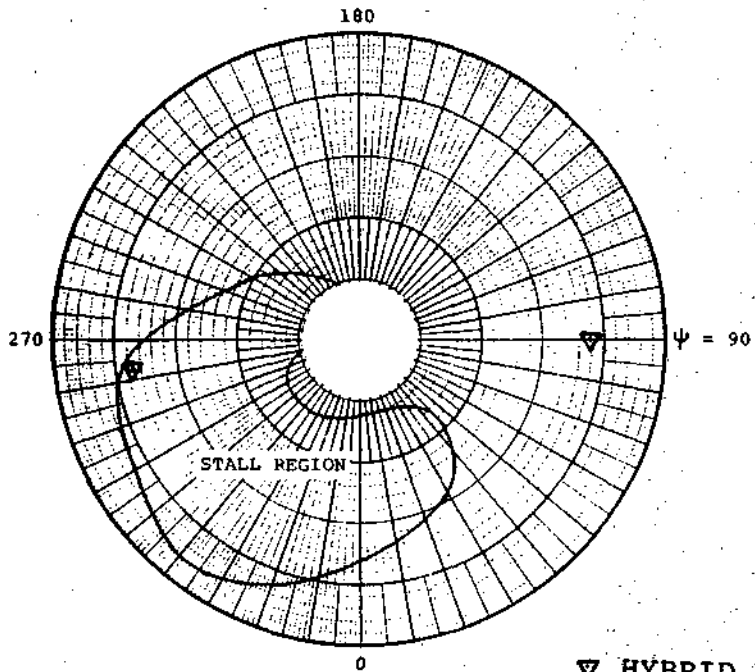
Notes:
 V_{tip} = 400 FPS
 Radius = 4 Ft.
 No. of Blades = 3
 Lateral Cyclic = .14°
 Longitudinal Cyclic = 8.72°
 Shaft Angle = 1.66°
 C_T/σ = .090
 Run 31 T.P. 8

ROTOR STALLED REGIONS

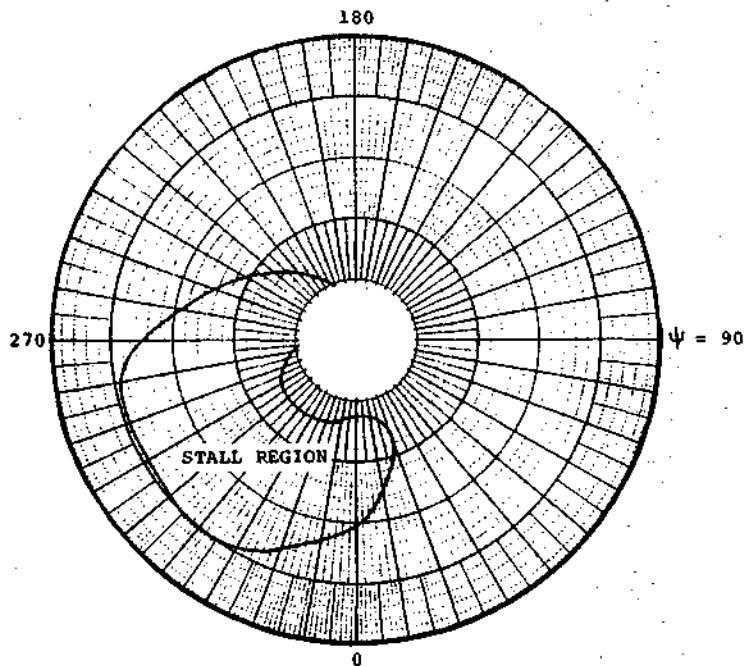
FIGURE 19

AT $\mu = .15$

LIFT STALL



MOMENT STALL

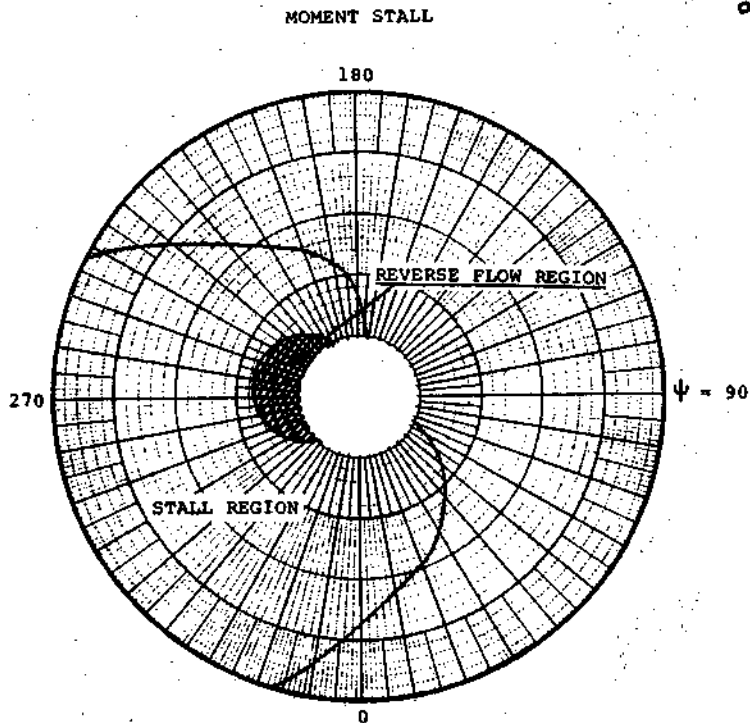
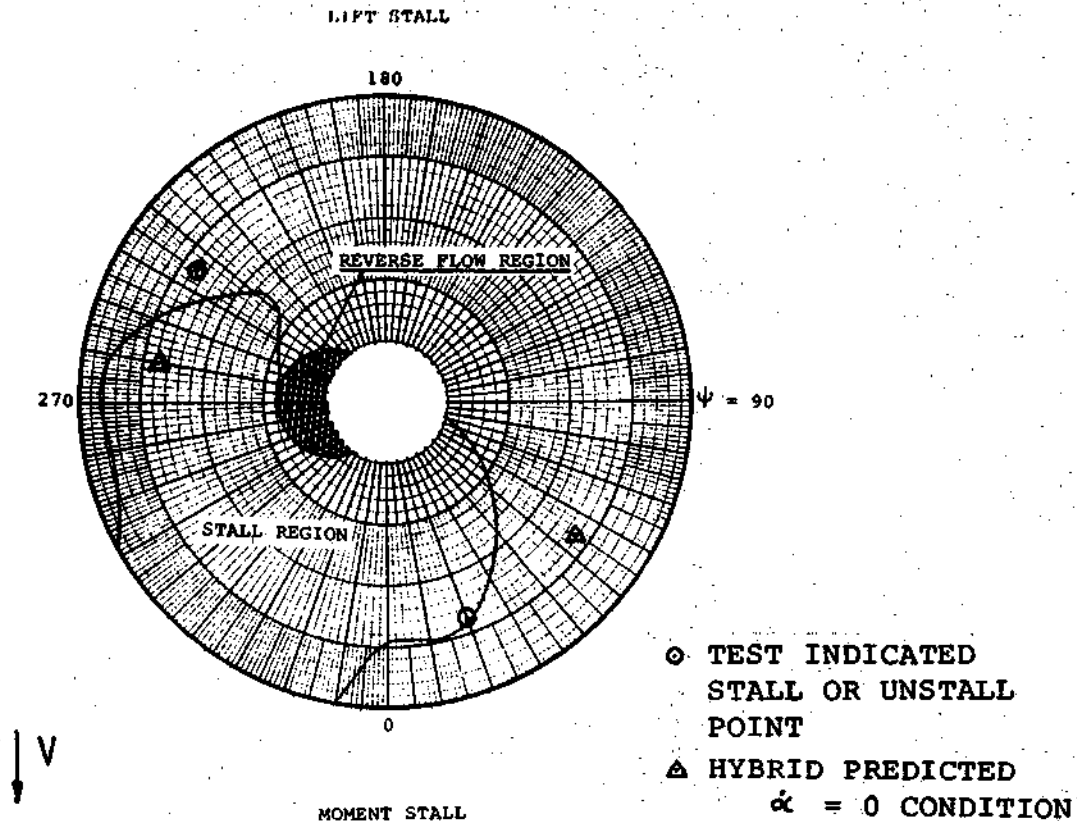


Notes:

$V_{Tip} = 250$ FPS
 Radius = 4 Ft.
 No. of Blades = 3
 Lateral Cyclic = $.20^\circ$
 Longitudinal Cyclic = 4.88°
 Shaft Angle = 4.88°
 $C_T/\sigma = .121$
 Run 18 T.P. 10

ROTOR STALLED REGIONS

AT $M = .35$



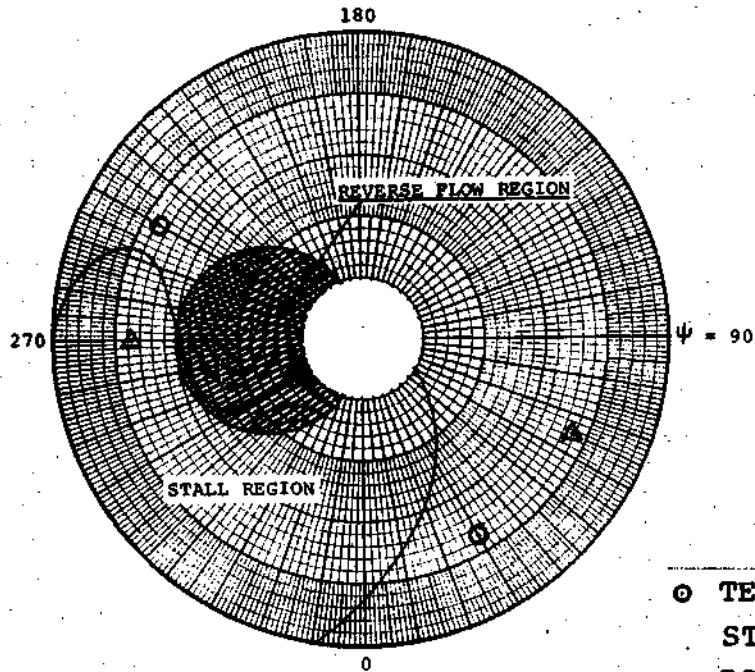
Notes:

- $V_{Tip} = 500$ FPS
- Radius = 4 Ft.
- No. of Blades = 3
- Lateral Cyclic = $.14^\circ$
- Longitudinal Cyclic = 4.89°
- Shaft Angle = -2.98°
- $C_T/\sigma = .133$
- Run 28 T.P. 12

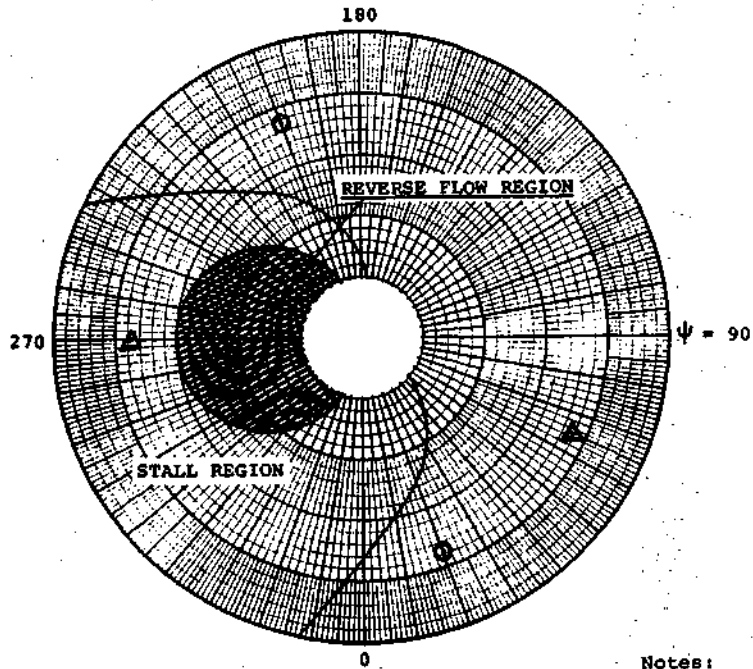
ROTOR STALLED REGIONS

AT $\mu = .60$

LIFT STALL



MOMENT STALL



Notes:
 $V_{Tip} = 400$ FPS
 Radius = 4 Ft.
 No. of Blades = 3
 Lateral Cyclic = $-.14^\circ$
 Longitudinal Cyclic = $-.8.7^\circ$
 Shaft Angle = 1.66°
 $C_T/\sigma = .090$
 Run 31 T.P. 8

of the time rate of change of α , therefore, is the prime consideration determining the azimuth location of the dynamic stall. As moment stall occurs on a portion of the blade, it develops an elastic pitching moment acting to oppose the increasing angle of attack. The rate of change of α is, therefore, reduced up to the point of lift stall and then to $\dot{\alpha} = 0$. As $\dot{\alpha}$ becomes negative, the airfoil experiences loads below statically predicted values. The manner in which the airfoil recovers from dynamic stall determines the damping characteristics of the airfoil.

A measure of the damping characteristics of an oscillating airfoil is obtained by investigation of curves of moment coefficient versus angle of attack. Reference 10 states that the net work done by an airfoil on the surrounding air is proportional to the area under such a curve, and is positive for a counterclockwise circuit and negative for a clockwise circuit. Thus, if the circuit encloses an area in a clockwise sense, it represents energy extracted from the airstream by the airfoil. Net energy extraction in a cycle (negative damping) implies that the rotor blade oscillation in which it occurred would tend to increase in amplitude.

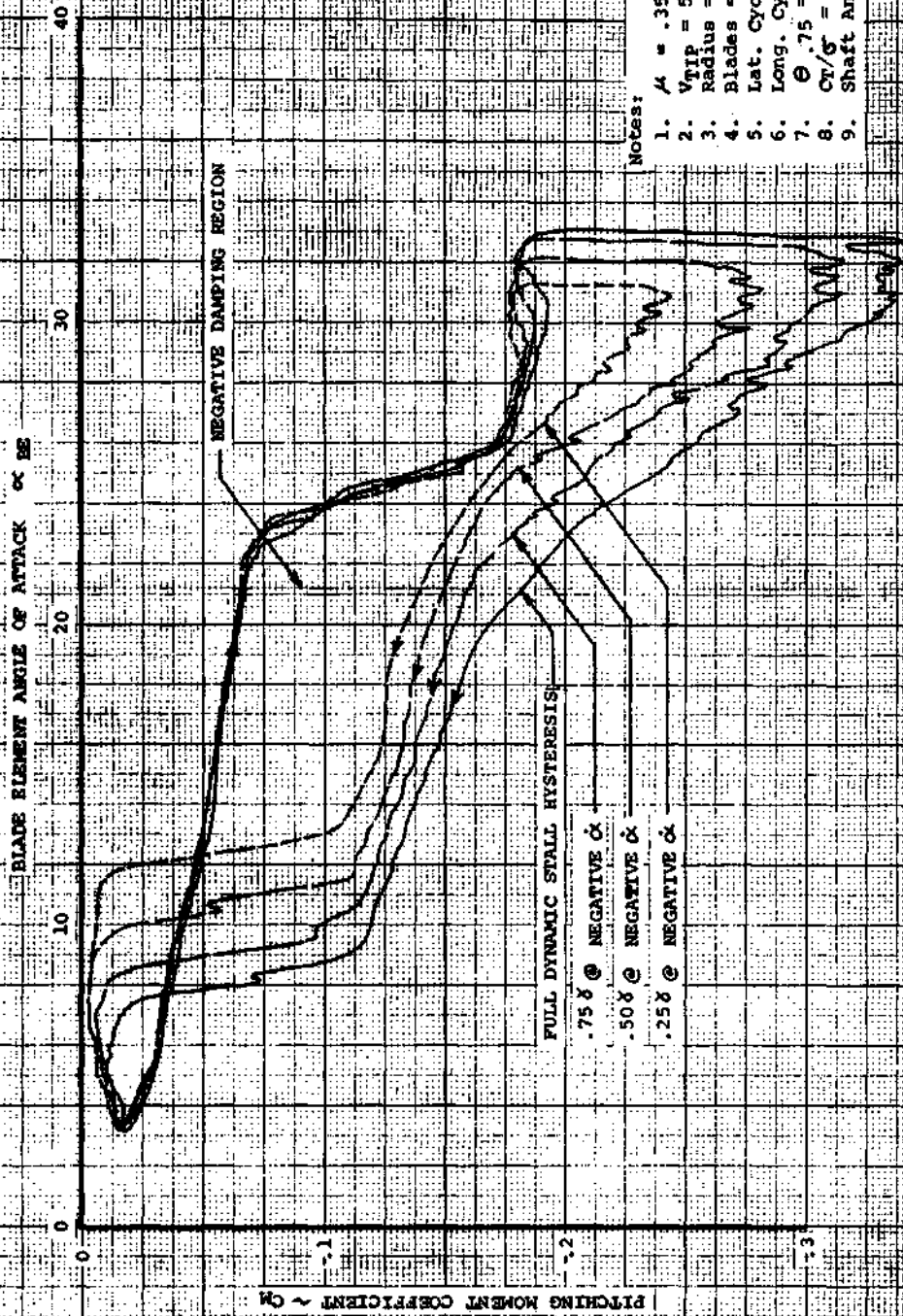
In order to visualize the effects of damping on rotor blade element airloads, a brief study was made using the hybrid simulation. In this study, the dynamic stall delay after $\dot{\alpha} = 0$, or the stall recovery, was varied by changing the γ function in the dynamic stall delay expression. Such changes were made only for the portion of the cycle experiencing negative $\dot{\alpha}$.

The pitching moment curves of Figures 22 and 23 represent rotor cycles with 25%, 50%, 75% and full dynamic stall hysteresis. The reduction in negative damping with decreasing stall hysteresis is evidenced by the reduction in area under the clockwise segment of the curve. The effects of improved damping characteristics are obvious in the curves of Figures 24 and 25. As the damping characteristics improve, negative pitching moment levels after stall decrease in magnitude, resulting in reduced elastic twist and, thereby, reduced blade root torsion. The blade element normal force level after stall increases and the overall flapping excursions are reduced. These effects seem to produce overall improvements in rotor performance and reductions in structural loads. Since the damping characteristics of a rotor operating in an unsteady environment are a function of the choice of airfoil,

PROJECT NO.
REPORT NO.
DATE

VERTICAL AIRCRAFT BOWING

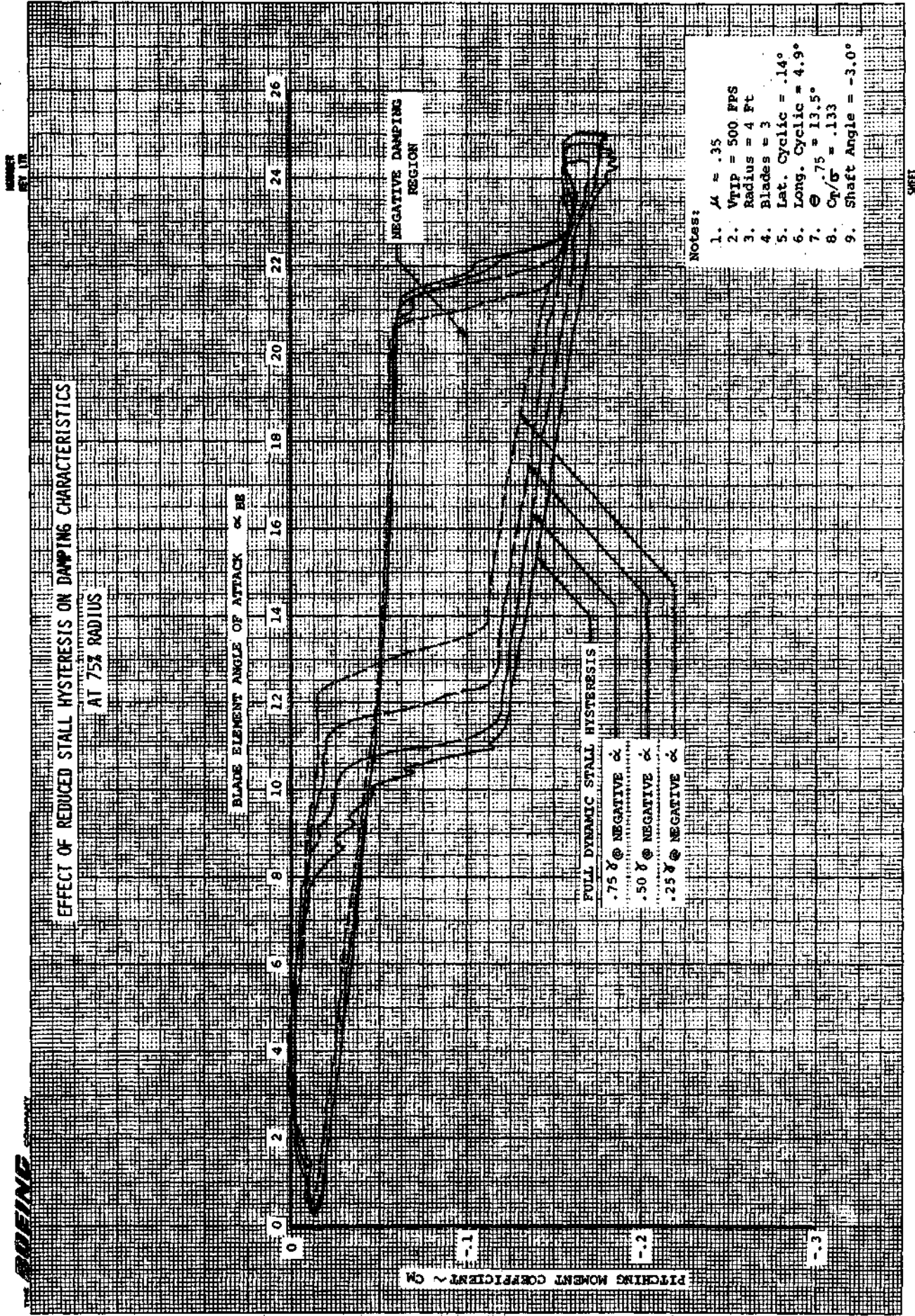
EFFECT OF REDUCED STALL Hysteresis ON DAMPING CHARACTERISTICS
AT 50% RADIUS



Notes:

1. $\mu = .35$
2. $V_{tip} = 500$ FPS
3. Radius = 4 Ft
4. Blades = 3
5. Lat. Cyclic = $.14^\circ$
6. Long. Cyclic = 4.9°
7. $\Theta = .75 = 13.5^\circ$
8. $C_T/C_D = .133$
9. Shaft Angle = -3.0°

PREPARED BY
CHECKED BY
DATE

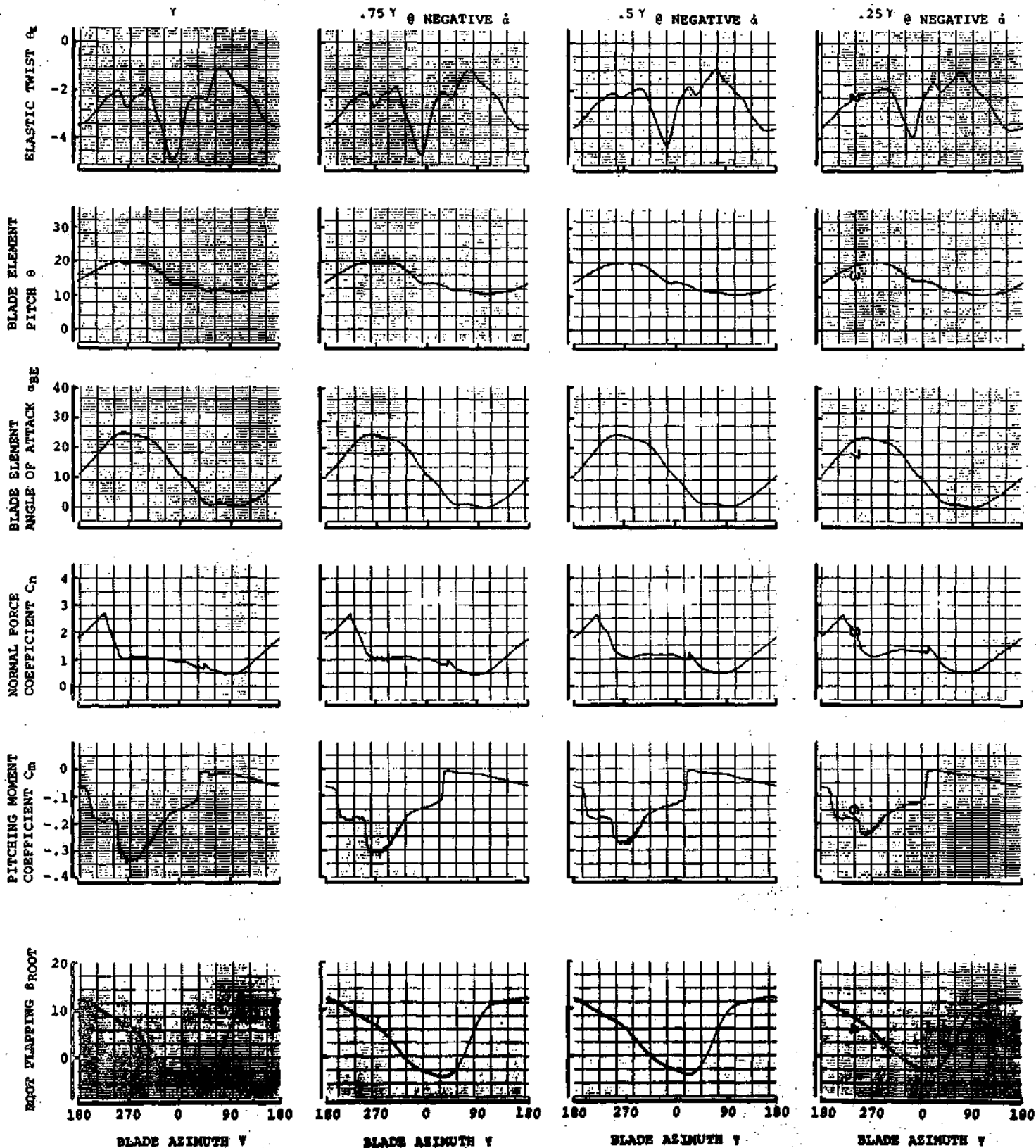


INFLUENCE OF VARIATIONS IN DYNAMIC STALL RECOVERY AT 50% RADIUS

$\mu = .35$

Notes:

- 1) $C_l = f(\alpha_{REF} C_{l1})$
- 2) $\alpha_{REF} C_{l1} = \alpha_{BE} - \gamma \sqrt{ka}$
- 3) $V_{Tip} = 500$ FPS
- 4) Radius = 4 Ft.
- 5) No. of Blades = 3
- 6) Lateral Cyclic = $-.14^\circ$
- 7) Longitudinal Cyclic = 4.89°
- 8) Shaft Angle = -2.98°
- 9) $C_T/\sigma = .133$
- 10) Run 28 T.P. 12

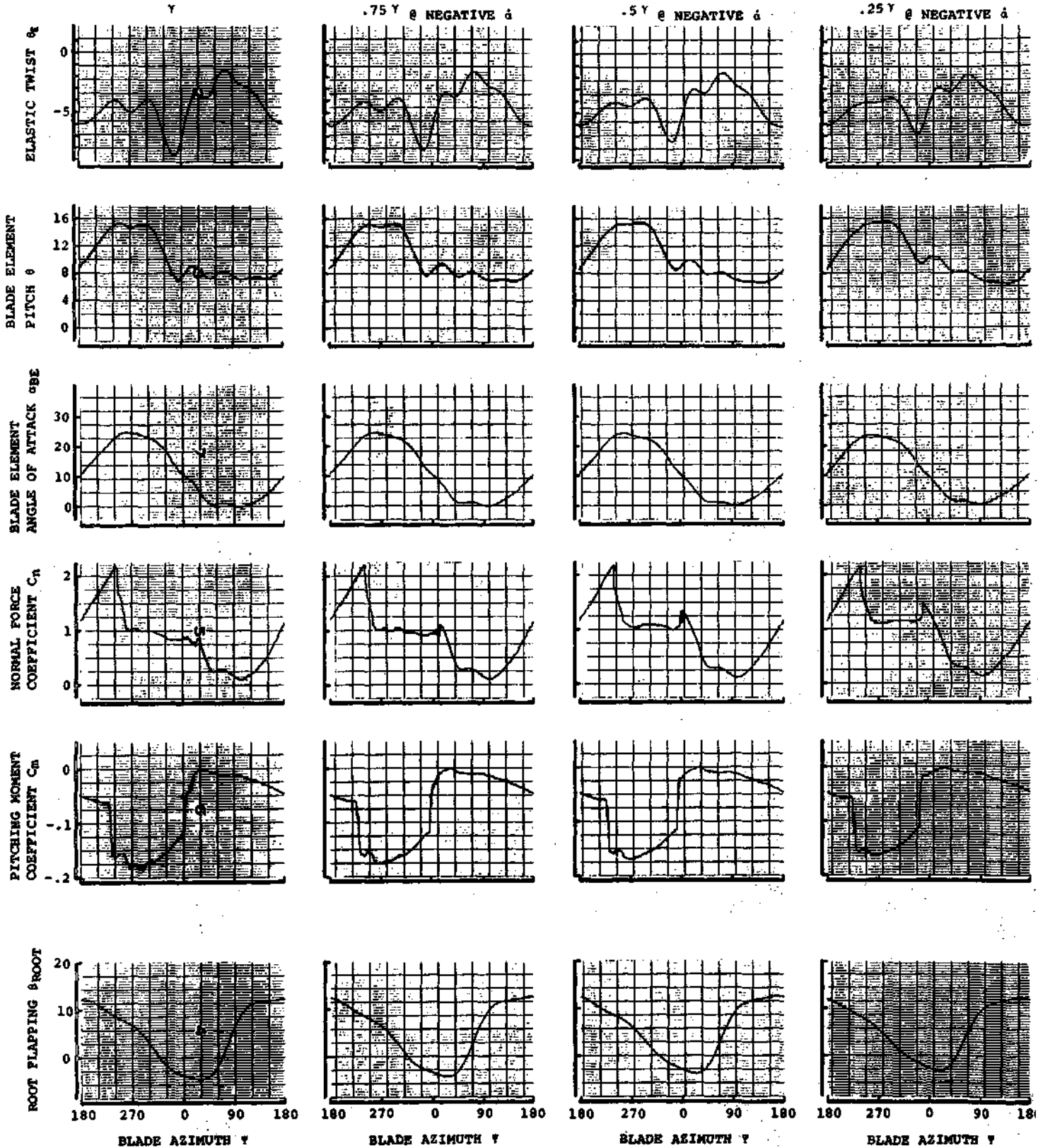


INFLUENCE OF
VARIATIONS IN DYNAMIC STALL RECOVERY
AT 75% RADIUS
 $\mu = .35$

FIGURE 25

Notes:

- 1) $C_1 = f(\alpha_{REF} C_1)$
- 2) $\alpha_{REF} C_1 = \alpha_{BE} - \gamma / K_d$
- 3) $V_{Tip} = 500$ FPS
- 4) Radius = 4 Ft.
- 5) No. of Blades = 3
- 6) Lateral Cyclic = $.14^\circ$
- 7) Longitudinal Cyclic = 4.9°
- 8) Shaft Angle = -2.98°
- 9) $C_T/\sigma = .133$
- 10) Run 28 T.P. 12



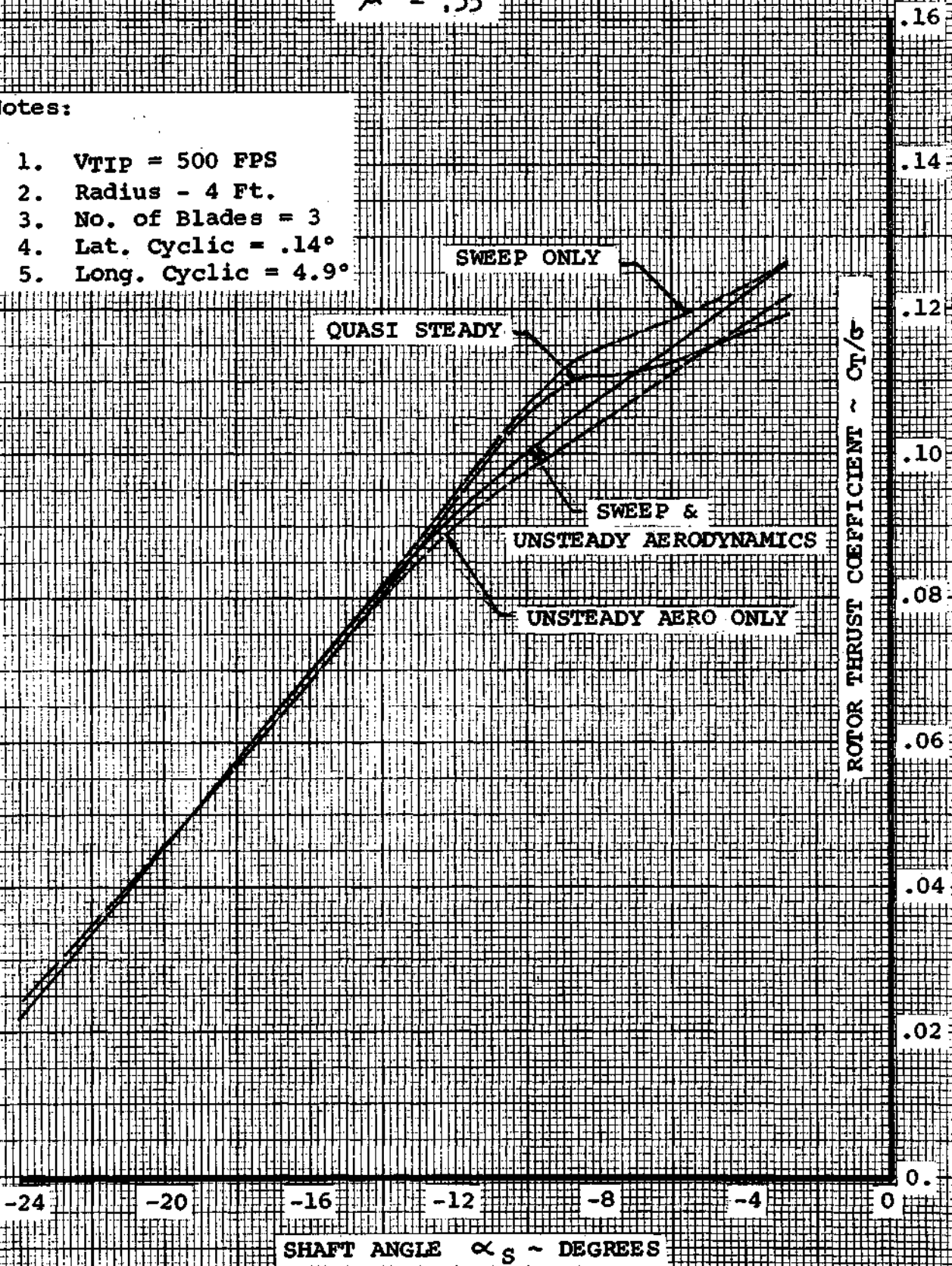
the question may be asked whether the characteristics of lift and moment stall recovery can be controlled by proper selection of airfoil without seriously affecting the favorable dynamic lift characteristics. Experimental evidence presented in Reference 12 indicates that favorable dynamic lift and pitching moment and recovery behavior can be obtained by choosing airfoils which do not display leading edge stall characteristics. Since trailing edge stall airfoils do not have the high $C_{l_{max}}$ characteristics typical of leading edge stall airfoils, a trade-off must exist between improved dynamic stall recovery characteristics and reduced two-dimensional lift capability.

To evaluate the contributions of the unsteady aerodynamics representation and the three-dimensional sweep effects within the present hybrid formulation, modifications to the present simulation were made to isolate each of these factors. Figures 26 through 29 present a summary of the results of these modifications for the advance ratios of .35 and .6. The quasi-static results were obtained by removing the sweep effects and unsteady aerodynamic effects from the formulation. Sweep effects were eliminated by removing the cosine of the sweep angle. Unsteady aerodynamic effects were eliminated by removing the γ function representation of the lift and moment overshoot, and setting the Theororsen terms $F = 1.0$, $G = 0$, eliminating the shed wake. A description of these terms is given in Reference 11.

CONTRIBUTIONS OF UNSTEADY AERODYNAMICS
AND THREE DIMENSIONAL EFFECTS AT
 $\mu = .35$

Notes:

1. VTIP = 500 FPS
2. Radius - 4 Ft.
3. No. of Blades = 3
4. Lat. Cyclic = .14°
5. Long. Cyclic = 4.9°



EUGENE DIETZGEN CO.
MADE IN U. S. A.

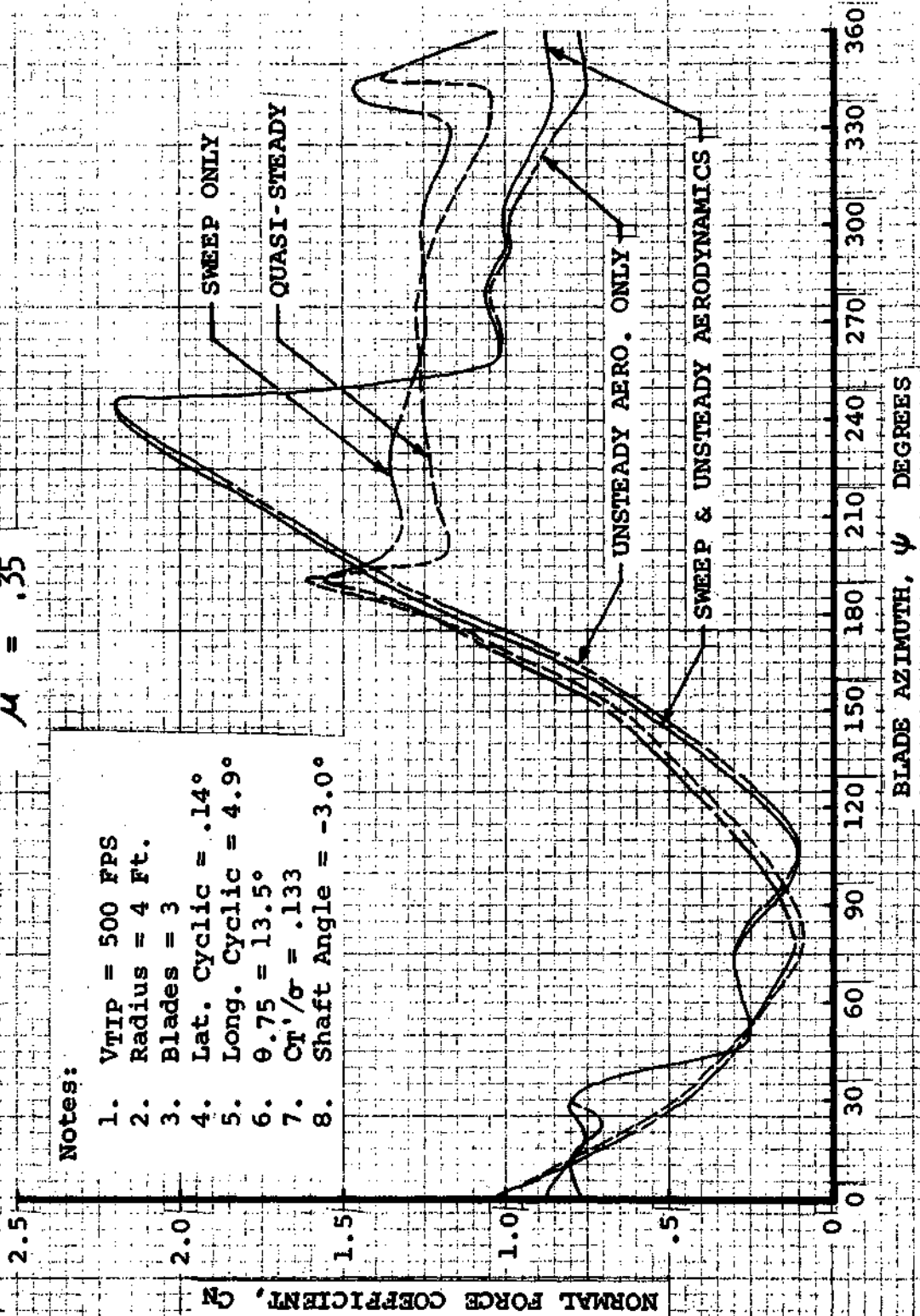
NO. 34DR-20 DIETZGEN GRAPH PAPER
20 X 20 PER INCH

CONTRIBUTIONS OF UNSTEADY AERODYNAMICS
AND THREE DIMENSIONAL EFFECTS AT

$M = .35$

Notes:

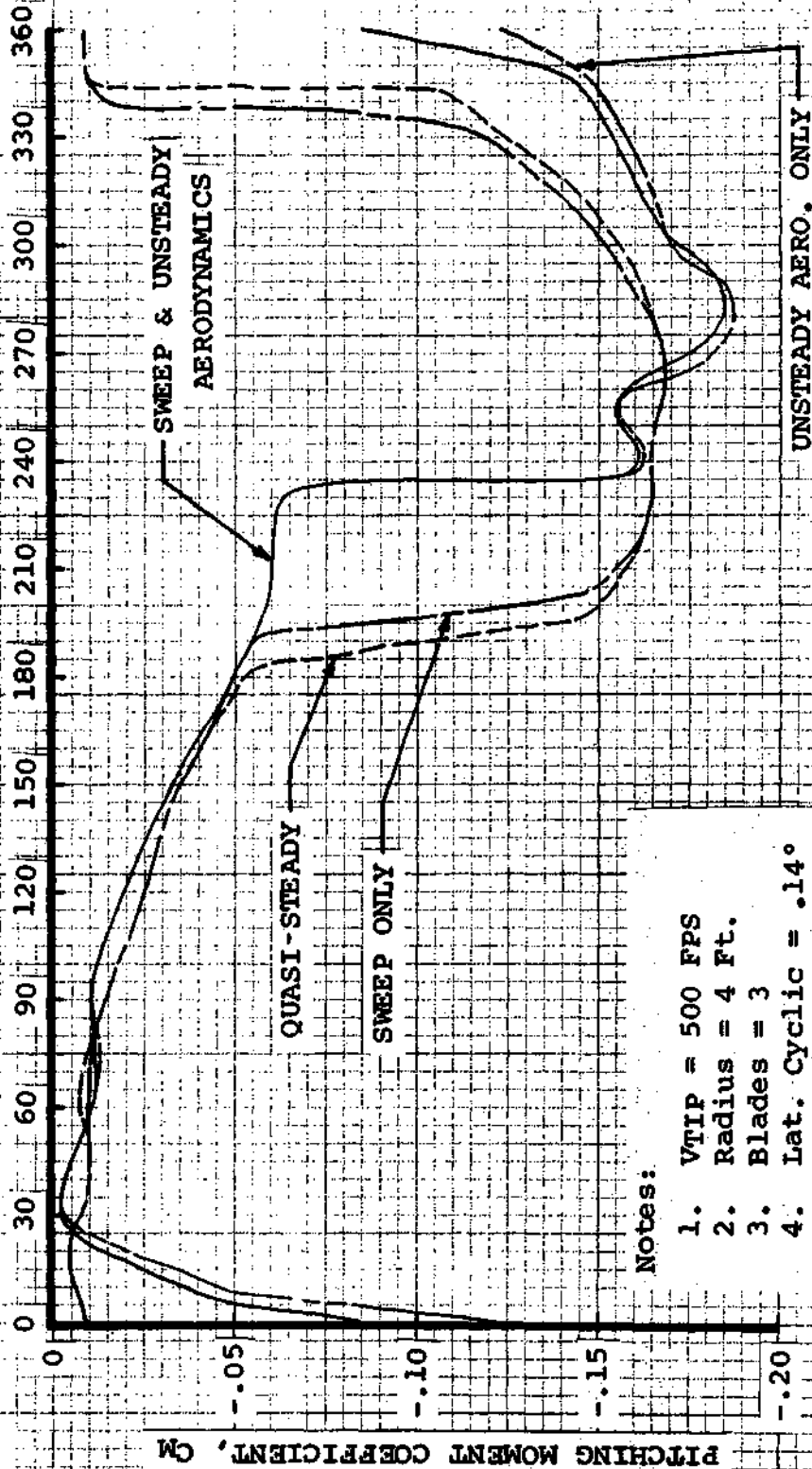
1. VTIP = 500 FPS
2. Radius = 4 Ft.
3. Blades = 3
4. Lat. Cyclic = $.14^\circ$
5. Long. Cyclic = 4.9°
6. $\rho = 0.75 = 13.5^\circ$
7. $C_T'/\sigma = .133$
8. Shaft Angle = -3.0°



**CONTRIBUTIONS OF UNSTEADY AERODYNAMICS
AND THREE DIMENSIONAL EFFECTS AT**

$\mu = .35$

BLADE AZIMUTH, ψ DEGREES



Notes:

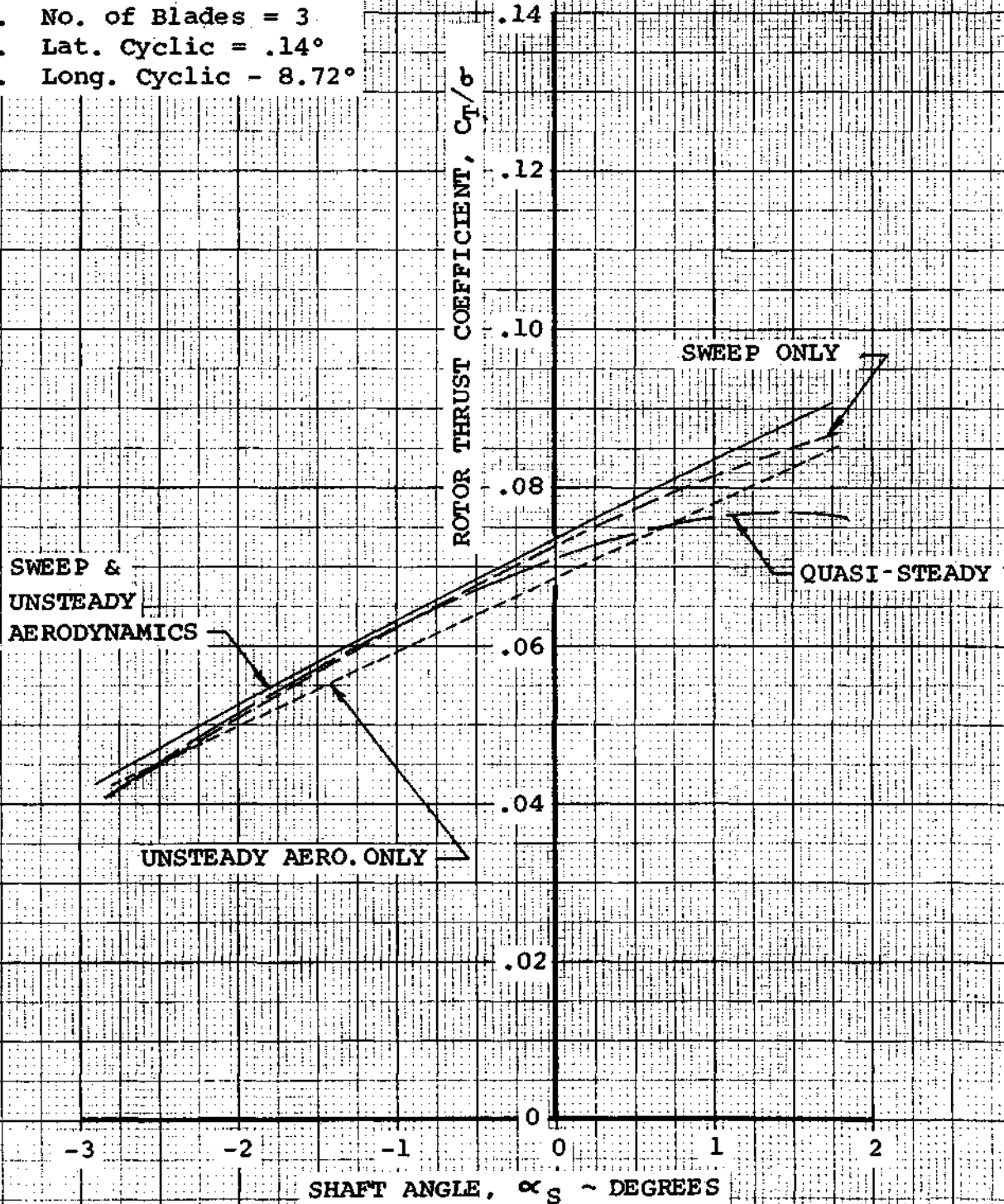
1. VTIP = 500 FPS
2. Radius = 4 Ft.
3. Blades = 3
4. Lat. Cyclic = $.14^\circ$
5. Long. Cyclic = 4.9°
6. $\theta.75 = 13.5^\circ$
7. $C_t'/\sigma = .133$
8. Shaft Angle = -3.0°

CONTRIBUTIONS OF UNSTEADY AERODYNAMICS
AND THREE DIMENSIONAL EFFECTS AT

$\mu = .6$

Notes:

1. VTIP = 400 FPS
2. Radius = 4 Ft.
3. No. of Blades = 3
4. Lat. Cyclic = .14°
5. Long. Cyclic = 8.72°



EUGENE DIETZGEN CO.
MADE IN U. S. A.

BOEING 1401P-211 DIETZGEN GRAPH PAPER
20 X 20 PER INCH

CONCLUSIONS

1. Because of its inherent computational speed and "engineer in the loop" on line versatility, the hybrid simulation is a valuable tool for studying the complex rotor environment. This tool can lead to a more improved representation of rotor unsteady aerodynamics and to the development of dynamic design criteria for airfoils and blade elastic characteristics.
2. The improvement in prediction of blade flapping in the stall regime over typical digital formulations may be attributed to the increased number of radial computations inherent in the hybrid simulation. A study is suggested to investigate the influence of radial update capability on prediction capability.
3. The existing formulations of unsteady aerodynamics effects are based on oscillating airfoil data not representative of angle of attack oscillations experienced by the rotor. Studies into the effects of oscillating airfoil pitch amplitude on the theoretical unsteady aerodynamic γ function representation and the resulting effects on dynamic lift and moment should be made to improve existing theoretical methods.
4. Investigation of model rotor blade root torsion results indicates that due to the unsteady aerodynamic environment of the blade, the rotor produces airloads representative of a full scale Reynolds number environment.
5. Additional hybrid capability to represent nonuniform downwash is required to predict rotor performance and blade airloads at the lower advance ratios ($\mu = .15$).

REFERENCES

1. Fisher, R. K., Jr., Bobo, C. J., AN EXPERIMENTAL INVESTIGATION OF THE HELICOPTER ROTOR BLADE ELEMENT AIRLOADS ON A MODEL ROTOR IN THE BLADE STALL REGIME, NASA CR-114424, September 1971.
2. Harris, F. D., Tarzanin, F. J., Jr., ROTOR HIGH SPEED PERFORMANCE, THEORY VS TEST. JOURNAL OF AMERICAN HELICOPTER SOCIETY, July 1970.
3. Bobo, C. J., HYBRID FORMULATION OF ROTOR AIRLOADS AND PERFORMANCE ANALYSIS, Boeing Vertol Document D210-10511-1, August 1972.
4. Harris, F. D., ARTICULATED ROTOR BLADE FLAPPING MOTION AT LOW ADVANCE RATIO, JOURNAL OF AMERICAN HELICOPTER SOCIETY, January 1972.
5. Sewell, R., ROTOR AIRLOADS AND PERFORMANCE ANALYSIS WITH NONUNIFORM INDUCED INFLOW (Computer Program B-67) Boeing Vertol Document D8-0312 December 1967.
6. Tarzanin, F., Ranieri, J., AEROELASTIC ROTOR ANALYSIS C-60, Boeing Vertol Document D210-10378 unreleased.
7. Gormont, R. E., UNSTEADY AERODYNAMICS EFFECTS, USAAMRDL Technical Report, Contract DAAJ02-71-C-0045, July 1972, unreleased.
8. McCroskey, W. J., DYNAMIC STALL OF AIRFOILS AND HELICOPTER ROTORS, Advisory Group for Aerospace Research and Development Paper, April 1972.
9. Gray, L., Liiva, J., Davenport, F. J., WIND TUNNEL TESTS OF THIN AIRFOILS OSCILLATING NEAR STALL, USAAVLABS TR 68-89A, Volume II.
10. Liiva, J., Davenport, F. J., Gray, L., Walton, I. C., TWO-DIMENSIONAL TESTS OF AIRFOILS OSCILLATING NEAR STALL, USAAVLABS TR 68-13A.
11. Bisplinghoff, R. L., Ashley, H., AEROELASTICITY, Addison-Wesley Publishing Company, Inc., Cambridge, Mass.

12. Olsen, John H., FLOW VISUALIZATION EXPERIMENTS ON PITCHING AIRFOILS, Boeing-Vertol Document D210-10450-1, December 1971.